

Temporal trends in methane emissions from a small eutrophic reservoir: the key role of a spring burst

Sarah Waldo^{1*}, Jake J. Beaulieu¹, William Barnett², D. Adam Balz³, Michael J. Vanni⁴, Tanner Williamson⁴, and John T. Walker⁵

¹Center for Environmental Measurements and Modeling, United States Environmental Protection Agency, Office of Research and Development, Cincinnati, 45268, USA

²Neptune and Company, Inc., Lakewood, 80215, USA

³Pegasus Technical Services, Cincinnati, 45268, USA

⁴Miami University, Department of Biology, Oxford, 45056, USA

⁵Center for Environmental Measurements and Modeling, United States Environmental Protection Agency, Office of Research and Development, Durham, 27709, USA

Correspondence to: Sarah Waldo (sahrwaldo@gmail.com)

*Currently at United States Environmental Protection Agency, Region 10, Seattle, 98101, USA

Abstract. Waters impounded behind dams (i.e. reservoirs) are important sources of greenhouse gases, especially methane (CH₄), but emission estimates are not well constrained due to high spatial and temporal variability, limitations in monitoring methods to characterize hot spot and hot moment emissions, and the limited number of studies that investigate diurnal, seasonal, and interannual patterns in emissions. In this study, we investigate the temporal patterns and biophysical drivers of CH₄ emissions from Acton Lake, a small eutrophic reservoir, using a combination of methods: eddy covariance monitoring, continuous warm-season ebullition measurements, spatial emission surveys, and measurements of key drivers of CH₄ production and emission. We used an artificial neural network to gap-fill the eddy covariance time series and to explore the relative importance of biophysical drivers on the inter-annual timescale. We combined spatial and temporal monitoring information to estimate annual whole-reservoir emissions. Acton Lake had cumulative areal emission rates of 45.6 ± 8.3 and 51.4 ± 4.3 g CH₄ m⁻² in 2017 and 2018, respectively, or 109 ± 14 and 123 ± 10 Mg CH₄ in 2017 and 2018 across the whole 2.4 km² area of the lake. The main difference between years was a period of elevated emissions lasting less than two weeks in the spring of 2018, which contributed 17% of the annual emissions in the shallow region of the reservoir. The spring burst coincided with a phytoplankton bloom, which was likely driven by favourable precipitation and temperature conditions in 2018 compared to 2017. Combining spatially extensive measurements with temporally continuous monitoring enabled us to quantify aspects of the spatial and temporal variability in CH₄ emission. We found that the relationships between CH₄ emissions and sediment T depended on location within the reservoir and observed a clear spatio-temporal offset in maximum CH₄ emissions as a function of reservoir depth. These findings suggest a strong spatial pattern in CH₄ biogeochemistry within this relatively small (2.4 km²) reservoir. In addressing the need for a better understanding of GHG emissions from reservoirs, there is a trade-off in intensive measurement of one water body versus short-term and/or spatially limited measurements in many water bodies. The insights from multi-year, continuous, spatially extensive studies like this one can be used to inform both the study design and emission upscaling from spatially or temporally limited results, specifically the importance of trophic status and intra-reservoir variability in assumptions about upscaling CH₄ emissions.

1 Introduction

40 Reservoirs are a globally important source of methane (CH₄) and other greenhouse gases (GHG) to the atmosphere, with recent estimates attributing 773 Tg carbon dioxide equivalents (CO₂-e) per year to reservoir surface emissions, nearly 80% as CH₄ (Deemer et al., 2016). The dominance of CH₄ in reservoir GHG budgets is due to the combination of gross CH₄ emissions and methane's large warming potential relative to CO₂. Reservoir CH₄ emissions have been estimated to be equivalent to roughly half of the global CH₄ burden from rice cultivation (~1200 Tg CO₂-e yr⁻¹, Ciais et al., 2013). Inland waters (lakes, rivers, and
45 reservoirs) can be hot spots for decomposition of organic matter, and respiration from these waters globally may offset the terrestrial carbon sink by up to 60% (Cole et al., 2007; Ciais et al., 2013). The carbon dynamics of reservoirs are of special interest for several reasons. Reservoirs generally receive more sediment input (hence organic C) from their watershed than comparable lakes, as they tend to be located lower in the landscape and have a larger ratio of catchment area to surface area (Hayes et al., 2017). Reservoirs also tend to drain watersheds with more agricultural or urban land use than the natural lake
50 watersheds (Thornton et al., 1990). The distribution of lakes and reservoirs across the United States is such that in many parts of the country total lentic surface area is dominated by reservoirs. Furthermore, emissions from reservoirs are considered anthropogenic and thus should be included in national greenhouse gas (GHG) emission inventories reported to the United Nations (Lovelock et al., 2019).

Emissions of GHGs from reservoirs are highly variable in space and time, making reservoir GHG budgets difficult to constrain.
55 This is especially true for CH₄, the production and emission pathways of which are highly dynamic. One key production pathway of CH₄ in water bodies is methanogenesis in anoxic sediment. Some of this CH₄ dissolves into the water column where it may be oxidized into CO₂ by methanotrophs or may diffuse to the atmosphere. Methane may also accumulate as bubbles in the sediment until the buoyant force of the gas bubble overcomes the overlying static pressure. The rate of this CH₄ bubbling, or ebullition, is affected by several biological and physical factors including carbon substrate availability, sediment temperature, oxygen availability, turbulence, and overlying pressure (Tuser et al., 2017). Thus, ebullition is highly variable in space and
60 time (Wik et al., 2016). Another potentially important source of CH₄ is production in oxic surface water, considered a "paradox" until recently (Schmidt and Conrad 1993; Grossart et al., 2011; Tang et al., 2014, 2016; DelSontro et al., 2018). The rate of diffusive flux from surface waters can be highly dynamic as it depends on the balance between production and emission (Hartmann et al., 2020).

65 Although the body of knowledge on CH₄ emissions from inland waters has grown considerably over the past decades, the high degree of spatial and temporal variability in emissions, coupled with limitations in monitoring methods, mean that many questions about reservoir emission behaviour remain. Recent studies have highlighted the importance of interannual patterns (Room et al., 2014), seasonal patterns (Yvon-Durocher et al., 2014), diurnal patterns (Podgrajsek et al., 2014; Deshmukh et al., 2014), sub-daily pulse events (Zhang et al., 2021), lake-zone spatial patterns (Juutinen et al., 2009; DelSontro et al., 2011; Maeck et al., 2013; McClure et al., 2020), and the relative contributions of hot-spots (Wik et al., 2016; Beaulieu et al. 2016), hot-moments (Bastien et al., 2011; Demarty et al., 2011; Jammot et al., 2015; Beaulieu et al., 2018; Harrison et al., 2018), and food web dynamics (Bartosiewicz et al., 2021; Grasset et al., 2018) in accurately characterizing lake and reservoir CH₄ emissions. Under-sampling in irregular systems leads to underestimation (Wik et al., 2016). The synthesis by Deemer et al. (2016) showed that reservoir GHG emission studies using spatially integrated methods reported higher F_{CH₄} than studies using

75 survey methods. Despite the need to better capture the spatiotemporal dynamics of reservoir CH₄ fluxes (F_{CH_4}) and its drivers, most monitoring studies to date have used survey methods that are often short-term, intermittent, and/or spatially limited. Use of micrometeorological methods such as eddy covariance (EC) to monitor reservoir F_{CH_4} can address many of the monitoring challenges by providing pseudo-continuous, long-term, spatially integrated flux measurements. A low-power open-path CH₄ sensor capable of making measurements for EC has only been available since circa 2011 (McDermitt et al., 2011), and using micrometeorological techniques to measure fluxes over open water (vs. land) can be difficult due to siting, footprint, and boundary layer turbulence considerations (Kenny et al., 2017, Higgins et al., 2013, Sahlee et al., 2014). Thus, relatively few studies have used EC to characterize F_{CH_4} over inland waters (Jammet et al., 2015, Jammet et al. 2017, Deshmukh et al., 2014, Eugster et al., 2011, Schubert et al., 2012, Podgrajsek et al., 2014a, Podgrasek et al., 2014b, Beaulieu et al., 2018). Further highlighting the scarcity of studies using this technique, the recent FLUXNET-CH₄ synthesis (Knox et al., 2019) of long-term (>1 year) EC monitoring of F_{CH_4} had only two open water sites among the 60 included. To our knowledge, this study is only the second to report pseudo-continuous, multi-year F_{CH_4} results over open-water, and the first to report long-term F_{CH_4} over open-water in a temperate region, for a eutrophic system, and for a reservoir.

This study reports the results of two years of pseudo-continuous (via EC and active funnel traps for ebullition), spatially extensive (via spatially-balanced CH₄ emission surveys) measurements of F_{CH_4} and key drivers of CH₄ production and emission. We organize our findings around two questions that can inform both the design of future monitoring studies and emission upscaling from limited results: (1) How important can interannual and intra-lake variability be in a single reservoir, and what causes it? (2) What does this tell us about how limited monitoring resources can best be used to constrain reservoir methane emissions?

2. Methods

95 2.1 Site description

Acton Lake is a small hypereutrophic reservoir located in southwestern Ohio (39.57 N, 84.74 W, 262 masl, Fig. 1a). The dam was constructed in 1956 and the reservoir and surrounding state park have been managed by the Ohio Department of Natural Resources since 1957. The reservoir's surface area is 2.4 km², it has a maximum depth of ~8 m, and the area near the dam undergoes thermal stratification in the summer. Although Acton Lake is immediately surrounded by a forested state park, land use in its watershed is >80% agricultural, with the majority used for intensive row cropping (Renwick et al., 2018). We used four main methods to monitor CH₄ fluxes (F_{CH_4}) from Acton Lake during 2017 and 2018: (1) the EC technique, (2) continuous ebullition monitoring with active funnel traps, (3) bi-weekly chamber measurements of diffusive emissions, and (4) spatially extensive surveys. The locations of the EC tower sites, active funnel trap/bi-weekly chamber measurement sites, and spatially extensive survey sites are depicted in Fig. 1a; the cumulative footprint probability distribution of the two flux tower sites is shown in Fig. 1b. The EC instrumentation was sited in the shallow region of Acton Lake due to logistical constraints related to both tower installation and boat traffic in the reservoir. How the methods were used in this study is summarized in Table S1. We used auxiliary meteorological and limnological measurements from stream gauging stations, a weather station, and thermistor string maintained by the Miami University (Renwick et al. 2018; Andersen et al. 2020), the locations of which are also shown in Fig. 1a.

110 2.2 Eddy covariance flux measurements

This site is registered as AmeriFlux site US-Act; information about the site as well as the flux data presented in this study are available online (<https://ameriflux.lbl.gov/sites/siteinfo/US-Act>). The EC instrumentation consisted of an ultrasonic anemometer to measure 3-D wind speed and direction (Model 81000, R.M. Young Company, Traverse City, MI, USA) and open path infrared gas analyzers (IRGAs) for measuring the number density of CH₄ (LI-7700), and CO₂ and water vapor (LI-7500A, LiCor Biosciences, Lincoln, NE, USA). The EC data streams were recorded at 10-Hz by a data logger (LI-7550, LiCor Biosciences, Lincoln, NE, USA), which was also equipped with a temperature sensor and a pressure transducer. The EC system was deployed from a dock piling 20 m from the northwestern shore of Acton Lake from 1 February 2017 thru 14 April 2018 (“EC S-1” in Fig. 1). The instruments were brought to the lab for calibration and maintenance on 15 April 2018, then redeployed on a tower installed into the reservoir sediment in the northeast corner of the reservoir on 5 May 2018 (“EC S-2” in Fig. 1). The system was shut down on 1 December 2018. Images of the EC system at each deployment location are included in the SI (Fig. S1). In addition to the EC setup, the flux tower was equipped with a net radiometer (NRLite2, Kipp and Zonen, Delft, The Netherlands), a cellular modem for remote communication (AirLink, Campbell Scientific, Logan, UT, USA), and a time-lapse camera (WCT-00125 TimelapseCam, WingScapes, Calera, AL, USA). The time-lapse camera was used to determine periods of ice cover. The system was powered by solar panels and a battery bank regulated via a solar charge controller (SunSaver, Morningstar Corporation, Newtown, PA, USA). All components of the EC system were run on a 12V system until relocation to the aquatic tower, when the EC setup (LI-7700, LI-7500A, RMYoung, and LI-7500) was retrofitted to run on 24V.

The raw 10-Hz EC data was processed into 30-minute fluxes using the software EddyPro v. 6.2 (Licor Biosciences, Lincoln, NE, USA). We used measurements of water depth from the Miami University weather station to determine instrument height above water surface on an hourly timestep, integrated into the flux processing as a dynamic metadata file. Additional processing steps followed community standards and included filtering the 10 Hz CO₂ measurements when CO₂ signal strength was <70, double coordinate rotation, block averaging, time lag compensation using covariance maximization, WPL density correction (Webb et al., 1980), and correction for high-pass and low-pass filtering effects (Moncrieff et al., 2004; Moncrieff et al., 1997). The area contributing to the measured flux was characterized for both sites using the online two-dimensional flux-footprint prediction tool (Kljun et al., 2015). We used R for postprocessing, and the code is available on GitHub (<https://github.com/USEPA/actonEC>). The 30-minute fluxes were rejected when the period did not pass the tests for stationarity and developed turbulent conditions (QC level 2 per the integrated scale of Foken et al., 2004). EC S-1 fluxes were further filtered for periods when winds were from the shore (between 195° and 330°); at EC S-2 we filtered for periods of low turbulence using a friction velocity (u_{star}) threshold of 0.07 m s⁻¹, based on the site-specific relationship between u_{star} and fluxes of CH₄ and CO₂ (Aubinet et al., 2012). We did not use u_{star} filtering at EC-S1 because the temporal coverage was insufficient to determine a u_{star} threshold. We define “acceptable” data or “acceptance rate” as those data meeting the EC QA/QC requirements, while “data coverage” includes non-operability due to power or instrument failures.

The overall EC F_{CH₄} data acceptance rate for the two-year monitoring period (26 January 2017 – 13 November 2018) was 31.3% (Fig. S2). In 2017, the data acceptance rate was lower, 23.4%, due to power issues and the need to filter for wind direction at the near shore EC S-1 site where the instrumentation was located for the whole year vs. 39.8% in 2018 when the instrumentation was relocated in the spring to the mid- reservoir EC S-2 site. The data coverage for the period of monitoring

from EC S-2 (May thru November) was 52.8%. Re-siting removed the need to filter periods based on wind direction and coincided with an improvement to the battery system that reduced incidences of power failure. At EC S-1, non-operability of the LI7700 due to power loss or other issues caused the majority of data rejection (40.4% of total monitoring periods), followed by filtering for wind direction (28.1%), and quality control filtering (7.8%). At EC S-2, power loss caused the majority of gaps (36.3%), followed by quality control filtering (16.6%).

2.3 Active funnel trap ebullition measurements

The active funnel traps (AFT) were based on the design of Varadharajan et al. (2010) and have been previously described by Beaulieu et al. (2018). Briefly, they consisted of a 0.3 m² funnel attached to a rigid tubing gas collection chamber equipped with a differential pressure sensor to monitor accumulated gas volume on a 5-minute timestep. We modified the Varadharajan design by incorporating siphons that auto-purge the collected bubble gas and refill the tubing volume with water. This modification keeps the AFTs from becoming filled with gas, allowing them to make useful measurements for longer periods of time. Trap gas samples were collected bi-weekly and analysed via a gas chromatograph equipped with a flame ionization detector (Bruker 450 GC, USA) to determine the composition of the bubble gas. The active trap data reduction followed the method described in Varadharajan et al. (2010) and Varadharajan and Hemond (2012). Circuit calibration to determine the relationship between voltage and height was performed pre- and post-trap deployment in the 2017 field season, and post-deployment in the 2018 field season. The volume of gas in the trap is calculated as:

$$AFT_{vol} = (Circ_{volt} * m + b) * \pi * \frac{AFT_d^2}{2} \quad (1)$$

where AFT_{vol} is the volume of gas in the funnel trap, $Circ_{volt}$ is the voltage output from the differential pressure sensor, m and b are the sensor-specific laboratory calibration multiplier and offset coefficients, and AFT_d is the diameter of the funnel tubing. We used a 12-point moving average (60 min) to smooth the gas volumes and minimize noise. Periods with known issues were filtered out of the dataset (e.g. power issues, trap drift from target location, etc.), as were large negative fluxes that reflected siphon purges. Following Varadharajan and Hemond (2012), we calculated fluxes on multiple time-bin widths (30-min, 1, 2, 6, 12, 24, 48 hr) but used the 2-hr rolling timestep for calculating the flux used in our final analysis:

$$F_{CH4_{eb}} = \frac{AFT_{vol}[CH_4]}{(T_f - T_i)A_F} \quad (2)$$

where AFT_{vol} is the volume of gas in the trap (l), $[CH_4]$ is the CH₄ concentration in the bubble gas (mg CH₄ l⁻¹), $T_f - T_i$ is the elapsed time (s), and A_F is the cross-sectional area of the funnel (m²). The AFT data reduction was performed in R and the scripts are available online (<https://github.com/USEPA/actonEC>).

The AFTs were deployed in late spring and retrieved in the fall each year. The shallow AFT (U-14) monitored ebullition from May 9 – October 3 in 2017, and from June 6 – December 11 in 2018. The deep AFT (U-12) monitored ebullition from May 10 – October 30 in 2017, and from May 24 – November 9 2018.

2.4 Chamber diffusion measurements

Diffusive F_{CH_4} was measured with a floating chamber biweekly at two sites during the field season. We used a rectangular, round-ended aluminum chamber with external polyvinyl chloride floats and a headspace fan, based on the CSIRO chamber

described in Zhao et al. (2015). An ultra-portable greenhouse gas analyzer (UGGA, PN: 915-0011, ABB, Los Gatos, CA) monitored the change in CH₄ mixing ratio in the chamber headspace over the duration of the chamber deployment (> 1 - 5 min), measuring at 1Hz and recording an averaged measurement every 5 s. We monitored the real-time UGGA time series to prevent ebullitive emissions from overwhelming the diffusive emission measurements. If a spike in CH₄ concentration was detected, we re-set the chamber. The floating chamber data reduction method has been described in detail in Beaulieu et al. (2016). Briefly, we used the following equation to calculate diffusive fluxes (moles m⁻² s⁻¹):

$$F_{\text{gas},D} = \frac{d\chi_{\text{gas}}}{dt} \left(\frac{V}{A} \right) \left(\frac{P}{RT} \right) \quad (3)$$

where $d\chi_{\text{gas}}/dt$ is the rate of change of the mixing ratio of CH₄ in the chamber headspace (ppm s⁻¹), V is the chamber volume (m³), A is the chamber surface area (m²), P is the pressure in the chamber headspace, R is the universal gas constant, and T is the temperature in the chamber headspace. The rate of change $d\chi_{\text{gas}}/dt$ for each chamber deployment was determined via fitting linear and non-linear models to the dataset and using Akaike information criterion (AIC) to choose the more appropriate model. Only models with an $r^2 > 0.9$ were retained. Data analysis and reduction was performed using R, and the scripts are available online (<https://github.com/USEPA/actonEC>).

Biweekly chamber monitoring was conducted from May 10 to December 11 in 2017, and from May 18 to October to December 13 in 2018. Note that the chamber monitoring began earlier and ended later than the AFT monitoring each year, due to technical issues with the AFTs.

2.5 Water measurements

Water temperature depth profiles were recorded continuously at two sites close to U-14 and U-12 (Fig. 1) using thermistors. At the shallow site (U-14) a string of seven thermistors (RBRsoloT, RBR Ltd., Ottawa, ON, Canada) were deployed at 0.1, 0.25, 0.5, 0.75, 1, 1.5 m below the air-water interface and at the sediment-water interface. We used this temperature profile to characterize water column stability in the footprint of the EC flux measurements based on the Brunt-Vaisala buoyancy frequency using the R package rLakeAnalyzer (Winslow et al., 2019). The Brunt-Vaisala buoyancy frequency was used as to indicate water column stability. It represents the frequency at which a parcel of fluid will oscillate when displaced vertically, a measure of resistance to mixing. A high oscillation frequency indicates strong resistance to mixing, whereas a low frequency indicates little resistance to mixing. At the deep site (U-12), sondes measuring temperature (Pro ODO, YSI Incorporated, Yellow Springs, OH, USA) were deployed at 0.1, 0.5, 1, 1.5, 2, 3, 4, 5, 6, 7, and 8 m below the air-water interface. Water temperature, specific conductivity, dissolved oxygen, pH, and chlorophyll a were measured biweekly with a YSI Multiparameter sonde at 0.1 and 1.5 m below surface at the shallow site (U-14), and 0.1, 1, 2, 3, 4, 5, 6, 7, and 8 m below surface at the deep site (U-12). Water samples for chlorophyll analysis were collected by Miami University near the reservoir inlet. Water samples were collected with an integrated tube sampler from the water surface to the euphotic zone depth. Chlorophyll samples were collected on 1.0 μm glass fibre filters and frozen at -20°C in opaque containers until processed. They were extracted in 95% ethanol for 24 h and analysed with a TD-700 (Turner Designs, San Jose, CA, USA).

Dissolved gas surface and profile samples were collected biweekly from both U-12 and U-14 using the headspace equilibration method. We collected water samples at depths of 0.1, 2, 4, 6, and 7 m at U-12 and at 0.1, 0.75, and 1.3 m at U-14. Using a 140-ml plastic syringe with a 2-way stopcock, we added 25 ml of ultra-high-purity helium to a syringe, then added 115 ml of sample water and agitated all samples for 5 minutes. We then transferred the headspace gas to pre-evacuated 12-ml glass vials topped

with a silicone-coated Teflon septum stacked on top of a chlorobutyl septa (Labco Ltd., UK). The headspace gas samples were analysed using gas chromatography (see section 2.3) to determine the CH₄ composition, and the dissolved CH₄ concentrations were calculated using measured headspace composition and the temperature-specific Bunsen solubility coefficients (Yamamoto et al., 1976). Full documentation of the calculations is available at the National Ecological Observatory Network's GitHub repository (<https://github.com/NEONScience/NEON-dissolved-gas>).

2.6 Whole-reservoir surveys

We conducted six surveys of Acton Lake over the summers of 2017 and 2018 to estimate whole-reservoir F_{CH₄}. The fifteen sample collection sites (Fig. 1, light blue circles), were determined using a generalized random tessellation survey (GRTS) design (Stevens and Olsen 2004; Olsen et al. 2012), a probability design that has been shown to reduce uncertainty relative to other designs (Beaulieu et al., 2016). At each site, we measured CH₄ diffusion, CH₄ ebullition, and surface water quality parameters. Survey measurements of diffusive F_{CH₄} were conducted with floating chambers in the same manner as described in section 2.4. Survey measurements of ebullitive F_{CH₄} were conducted with passive funnel traps (PFTs) deployed overnight (>15 hours). The PFTs are a simplified version of the AFTs described in section 2.3: they consist of a 0.3 m² funnel attached to a section of tubing for gas collection, but do not have a pressure sensor or siphon. Upon retrieval, the total time of deployment and total volume of gas in the tubing were recorded, and three 25 mL samples of the gas were collected for gas composition analysis via gas chromatograph (see section 2.3). Ebullitive F_{CH₄} from the PFTs was also calculated using Equation 2 (section 2.3), but the trap volume was determined by direct measurement of the collected gas, and T_f – T_i is defined as the deployment period. Dissolved gas sample collection and depth profiles of water quality parameters were taken at one deep site (U-12) and one shallow site (U-14) during each whole-reservoir survey. The surveys were initiated on 10 July 2017, 31 August 2017, 4 October 2017, 10 July 2018, 14 August 2018, and 20 September 2018, and concluded the following day.

2.7 Gap-filling and upscaling

We use the term “gap-filling” to refer to our method to determine values for missing observations in our measurement time series, while “upscaling” refers to the best estimate of whole-reservoir F_{CH₄}. For this analysis, we separated the year into different seasons, categorizing November thru March as “winter”, or the cold season, and May thru September as “summer”, or the warm season. We refer to April and October as the “shoulder” season. The spring burst period is defined as 24 May thru 4 June. For the EC timeseries, we developed an artificial neural network (ANN) to gap-fill 30-minute F_{CH₄} using predictor variables with biophysical links to CH₄ production and emission: sediment temperature (sedT), air temperature, latent heat flux (LE), sensible heat (H), wind speed, u_{star} (friction velocity, a measure of turbulence), photosynthetically active radiation, overlying static pressure, and change in static pressure, where static pressure is the sum of overlying atmospheric and hydrostatic pressure. We also included indicators for the tower location, hour of day, and day of year as drivers. Gaps in the sedT, air temperature, wind speed, wind direction, and static pressure time series were filled using observations from a nearby weather station. Gaps in LE, H, and u_{star} were gap filled using the mean diurnal course function from the R package REdyProc (Wutzler et al., 2019) on the 30-minute timestep. We used k-means clustering to assign ten clusters before selecting the training, testing, and validation datasets. The cluster assignments allowed us to select subsets with probabilities proportional to the

clusters, ensuring that the clusters were not over- or underrepresented as a result of the splits. We employed a selective ensemble approach to optimize the ANN model performance, using the R package `nnet` (Venables and Ripley, 2020). Each ANN ensemble included models with 5-20 layers and 50 different starting weights, for a total of 800 model results. The top 100 models were selected based on the testing R^2 results, then the median CH_4 value from the best 100 models was used as the predicted flux. To characterize both sampling and model uncertainty, we replicated this procedure with 20 resamplings of the data. For each half hourly F_{CH_4} we calculated the median predicted value of the best 100 models in each of the 20 ensembles of 800 models (c.f. Knox et al., 2016). Missing half hourly F_{CH_4} values were gap filled using the median of the medians from the 20 ensembles. ANN modelling and gap-filling was performed in R and the scripts are available online (Barnett et al., 2021). We gap-filled short gaps in the AFT continuous datasets using linear interpolation and calculated annual emissions via summing the daily observations. We gap-filled the biweekly chamber measurements of diffusive F_{CH_4} via linear interpolation. For periods at the start and end of the monitoring seasons with chamber measurements but no AFT measurements, we used the typical ratio between diffusive and ebullitive F_{CH_4} to estimate total F_{CH_4} for the site. We gap-filled the spatial survey measurements by interpolating between each of the three annual surveys. To estimate annual emission, we applied the F_{CH_4} value determined by the first survey of the year to every day between 1 May and the first survey, and the F_{CH_4} value determined by the last survey of the year out through 15 October. We assumed an F_{CH_4} of zero between 15 October and 1 May for both the spatial survey dataset and the AFT plus chamber datasets.

To upscale to whole-reservoir F_{CH_4} , we used a hybrid approach, combining results from EC, the deep-site (U-12) AFT, and the spatial surveys. We stratified Acton Lake into shallow (<3 m) and deep (≥ 3 m) areas and used reservoir bathymetry to determine the surface area for the shallow and deep portions: 0.8 km² and 1.6 km², respectively. The depth cut-off of 3 m roughly corresponds to the greatest depth of the EC footprint. We then used F_{CH_4} measured by EC to characterize the shallow portion of the reservoir. For the deep portion, we calculated the ratio (reservoir ratio, or RR) between the measured F_{CH_4} (ebullitive + diffusive) at the U-12 AFT (hereafter, deep AFT F_{CH_4}) and the mean of F_{CH_4} measured at the other deep sites (U-01, U-04, U-05, U-08, U-11, U-12, U-13, U-15, U-16, U-17, and U-18, see Fig. 1). We calculated this RR for each of the six spatial survey dates. To characterize F_{CH_4} in the deep portion of the reservoir, we applied the RR from the first survey to the deep AFT F_{CH_4} continuous timeseries data collected before 10 July 2017, and likewise applied the RR from the last survey to the timeseries data collected after 20 September 2018. For the periods in-between, we used linear interpolation to produce a daily RR and applied that to the deep AFT F_{CH_4} continuous timeseries. We weighted the cumulative shallow and deep CH_4 areal emissions by the shallow and deep fraction of the reservoir to determine the whole-reservoir CH_4 emissions. We refer to this estimate of whole-reservoir emissions as the “hybrid” upscaled estimate.

2.8 Uncertainty Analysis

We parameterized the uncertainty in the EC time series of F_{CH_4} using three different measures: the random measurement error, the bias error of the gap-filled dataset, and the 95% confidence intervals of the gap-filled dataset. The random measurement error is calculated from the variance of the covariance (Finkelstein and Sims, 2001), and reflects instrument noise, variation in footprint over a given 30-minute flux integration period, and the stochastic nature of turbulence. As described in Jammet et al., (2017), the random error decreases with increasing dataset size and is negligible at the resolution of cumulative annual fluxes but can be substantial for individual flux measurements (Richardson et al., 2006; Moncrieff et al., 1996). The random error was

290 calculated as part of the EddyPro processing, and we report the summary statistics in section 3.2. Unlike random errors, systematic biases can accumulate to affect the cumulative seasonal or annual flux. Although the measurement bias cannot be quantified, we calculated the systematic bias in the annual fluxes due to gap-filling following Moffat et al. (2007) and Jammet et al. (2017):

$$BE = \frac{1}{N} \sum (p_i - o_i) \quad (5)$$

295 where N is the number of values in the validation time series, p are the values predicted by the ANN, and o are the observed values in the validation time series. The bias error was multiplied by the total number of gap-filled values to obtain the total annual bias. We calculated the 95% confidence interval of the gap-filled dataset using the distribution of the 20 ANN medians extracted from the 20 resamplings, which consider both sample and model uncertainty (Knox et al., 2016).

We used root-sum-squared error propagation of the error in AFT_{vol} and $[CH_4]$ to characterize the uncertainty in ebullitive F_{CH_4} measured by the AFTs. Compared to error in AFT_{vol} , the error contribution from other terms in Eq. 2 was negligible. As described in Varadharajan et al. (2010), we propagated the error in m , offset, and electronic noise through Eq. 1, adding a 2-ml dead volume error each time the AFTs flushed to account for gas that could be trapped in the fittings at the top of the collection chamber. Our mean slope and slope error were similar to those reported in the Varadharajan methods paper (31 and 0.31, respectively, compared to 28 and 0.5); the mean (V_{zero}) and standard deviation (ΔV_{zero}) of the offset terms we used were slightly larger: 0.51V and 0.071V for the shallow site, 0.41V and 0.045V for the deep site (compared to 0.15 and 0.015); our calculated electronic noise (ΔV_{out}) was smaller (0.4 mV vs. 3 mV in Varadharajan), so we defaulted to their value. The standard deviation between the multiple trap gas samples was used as the uncertainty in $[CH_4]$. This term was generally small compared to the uncertainty due to AFT_{vol} error. The cumulative errors were propagated by summing in quadrature.

300 The whole- reservoir surveys provide an estimate of F_{CH_4} integrated across the entire reservoir surface area and a 95% confidence interval range (Beaulieu et al., 2016). Variance estimates calculated from GRTS incorporates spatial autocorrelation, if present, resulting in smaller uncertainty ranges than survey approaches that ignore spatial autocorrelation (Stevens and Olsen, 2003). The GRTS design and data reduction were executed in R using the `spsurvey` package (Kincaid et al., 2019). We propagated the cumulative uncertainties across 2017 and 2018 by taking the 95% confidence interval of each survey and summing them in quadrature.

315 The uncertainty in the hybrid approach to the upscaled cumulative whole-reservoir emissions were also determined by error propagation, combining the uncertainty in the deep AFT measurements, the spatial surveys, and the EC measurements.

2.9 Statistical and Quantitative Analysis

For these analyses, we used the non-gap-filled measurement time series. We quantified the relationship between sediment temperature ($sedT$) and F_{CH_4} using Q10 and breakpoint analyses. The concept of an “ecological Q10” (DelSontro et al., 2016) follows from the physiological exponential relationship between metabolic processes and temperature. In contrast to physiological Q10 values, ecological Q10, hereafter “ecoQ10” values are muddled by time-lags and competing rate enhancers and inhibitors (e.g. that temperature affects both methanogens and methanotrophs, Segers, 1998; Duc et al., 2010; Lofton et al., 2014). While the physiological Q10 value for methanogenesis converges around 4 (Yvon-Durocher et al., 2014), ecoQ10

325 values for methane fluxes have been reported to range from 1 – 35 (e.g. DelSontro et al., 2016; Wik et al., 2014; Duc et al., 2010). We calculated the ecological Q10 (DelSontro et al., 2016) using the equation:

$$ecoQ10 = 10^{10b} \quad (6)$$

where b is the slope of the regression between temperature and F_{CH_4} .

We also used a two-dimensional Kolmogorov-Smirnov test (2DKS, Garvey et al, 1998) to quantify the temperature breakpoint distinguishing winter conditions where F_{CH_4} is near zero and unrelated to temperature from warm weather conditions where F_{CH_4} is elevated and positively correlated with temperature. The 2DKS test is a non-parametric statistic that uses measures of disagreement to define the largest difference between cumulative distribution functions, that is, a threshold or breakpoint (Lopes et al., 2008). We applied the 2DKS test to each of the continuous F_{CH_4} monitoring datasets: EC, shallow AFT, and deep AFT, each for 2017 and 2018 for a total of six 2DKS tests.

We looked at diurnal patterns on monthly and daily timescales. For the monthly timescales we binned 30-minute periods and took the median. For daily timescales we adapted the methods used by Podgrajsek et al. (2014) to quantify “strong” diurnal patterns. For 24-hour periods with at least eight night-time and eight daytime non-gap filled 30-minute flux measurements, we compared the median of daytime F_{CH_4} to night-time F_{CH_4} . The period was defined as having a strong diurnal pattern if 1) 1) the difference between daytime vs night time F_{CH_4} median was >50 %, and 2) the contiguous points in the 30-minute times series were smooth, i.e. more similar than points separated in time. We determined smoothness using visual inspection.

340 We compared the cumulative F_{CH_4} measured from Acton Lake during each year of this study to output from the size-productivity model (Del Sontro et. al, 2018). This model uses the following equation to predict total CH_4 :

$$\log_{10}(total\ CH_4 + 1) = 0.778 * \log_{10}(chla) + 0.940 \quad (7)$$

where total CH_4 is in units of $mg\ C\ m^{-2}\ d^{-1}$, and *chla* is in units of $ug\ L^{-1}$.

345 3. Results

3.1 Temporal patterns in F_{CH_4}

We observed a consistent pattern of elevated F_{CH_4} during the warm season across all measurement methods (Fig. 2). In both monitoring years, the majority of cumulative total CH_4 emissions (>85%) occurred in the five-months between May 1 and September 30, when air and sediment temperatures were warmer (Fig. 4 (a)), and latent heat fluxes were elevated (Fig. 4 (b)). We observed larger-magnitude CH_4 emissions in 2018 relative to 2017 at Acton Lake across each observation type except for the deep site (Table 1). The EC and spatial survey results indicated similar warm-season mean fluxes in 2017: 9.73 ± 0.67 and $9.98 \pm 6.2\ mg\ CH_4\ m^{-2}\ hr^{-1}$. Results from both methods indicated larger-magnitude mean F_{CH_4} in 2018: $17.5 \pm 0.38\ mg\ CH_4\ m^{-2}\ hr^{-1}$ per the EC system and $13.0 \pm 6.6\ mg\ CH_4\ m^{-2}\ hr^{-1}$ per the spatial surveys (Table 1). Both the shallow site results also indicated elevated F_{CH_4} in 2018 relative to 2017, while the deep site results were effectively the same (Table 1). The lower-magnitude mean F_{CH_4} measured at the shallow site compared to the mean F_{CH_4} measured by EC is likely due to the under-representation of hot-spots (Wik et al., 2016). The wintertime F_{CH_4} measured by EC indicate that during the winter months F_{CH_4} dropped by more than an order of magnitude to a baseline close to zero: between 1 Nov and 1 April F_{CH_4} was $0.60 \pm 0.69\ mg\ CH_4\ m^{-2}\ hr^{-1}$. The surface of Acton Lake was frozen for several periods during the 2017-2018 winter: 27 Dec 2017-10 Jan 2018; 13-21 Jan 2018; and 5-15 Feb 2018, during which F_{CH_4} was $0.08 \pm 0.46\ mg\ CH_4\ m^{-2}\ hr^{-1}$.

360 The non-gap filled, quality filtered 30-minute F_{CH_4} measurements had a mean random error (\pm SD) of 1.3 ± 1.9 and 1.8 ± 1.7
mg CH_4 m^{-2} hr^{-1} in 2017 and 2018, respectively or 15.5% and 13.7% of the mean annual fluxes. The fractional errors were
larger in the winter months when F_{CH_4} was small (mean winter random error: 23%) and smaller during the warmer months
when F_{CH_4} was larger (mean summer random error: 15%). Both the magnitudes and patterns in the random errors are similar
to those observed by Jammet et al. (2017) in a subarctic aquatic ecosystem. Similarly, we found gap-filling our F_{CH_4} time series
365 with ANN worked well with a few exceptions. The median R^2 value for the 20 extractions was 0.79, and the cumulative bias
error was minimal: the 20 ANN extractions yielded a median bias of 0.25 (range of -3.7 to 3.5) g CH_4 m^{-2} , or up to 3.3%
of cumulative emissions over the two-year monitoring period. The ANN establishes non-linear predictive power to each of the
driver inputs, defined as a “Variable Importance Factor” (VIF) in terms of a percent importance to the predictive power of the
model. The median VIFs from the 20 ANN extractions are plotted in Fig 3; a consistently high ranking across runs indicates a
370 strong relationship with F_{CH_4} . The biophysical drivers with the highest variable importance were static pressure (the sum of
water pressure and air pressure), change in static pressure, and sediment temperature.

The most substantial difference between the two monitoring years is the period of elevated emissions in late May to early June
observed by the EC monitoring in 2018 but not 2017 (hereafter “spring burst”). We define the spring burst as the period from
24 May thru 4 June, where the daily average F_{CH_4} observed by EC was ≥ 25 mg CH_4 m^{-2} hr^{-1} . Maximum F_{CH_4} of 62.0 mg CH_4
375 m^{-2} hr^{-1} occurred on 29 May 2018. While the 2017 EC monitoring does indicate a small burst in F_{CH_4} of 20.4 mg CH_4 m^{-2} hr^{-1}
on 5 June, overall F_{CH_4} was much smaller: mean F_{CH_4} for 24 May - 4 June 2017 was 3.6 ± 1.8 mg CH_4 m^{-2} hr^{-1} . Although the
AFT at the shallow site was not operational during the spring burst, diffusive F_{CH_4} measurements indicate that F_{CH_4} was elevated
at that site compared to the deep site. Although none of the spatial surveys coincided with the spring burst period, the deep site
monitoring indicates that the spring burst did not extend to the deeper parts of the reservoir. The cumulative CH_4 emission over
380 the 2018 twelve-day spring burst period was 10.8 g CH_4 m^{-2} which is 15% of the cumulative annual emissions measured by
EC in 2018 (Table 1), and which accounts for 59% of the difference in the EC cumulative annual emissions between 2017 and
2018.

The differences between the 2017 and 2018 monitoring years continues past the early summer (Fig. 2, Fig. 4). During 2017,
 F_{CH_4} increased to a maximum in late summer, then declined back to the winter baseline. Maximum emissions at the deep site
385 in 2017 lagged and were dampened compared to the shallow site. In contrast, the 2018 summer and fall in the shallow portion
of the reservoir (EC and shallow site) were characterized by episodic emission pulses and declines before tapering down to the
winter baseline. The deep site emissions were in phase with the shallow site but did not have the same pulses. There was a late
season pulse at the deep site in 2018 that coincided with reservoir turnover (Fig. 4(g)), and a drop in dissolved CH_4 below the
thermocline at the deep site (Fig. S3).

390 We used the EC measurements of F_{CH_4} to look for diurnal patterns in emissions. We found that Acton Lake did not have a clear
over-arching diurnal pattern when aggregated over monthly timescales, (Fig. S4), but out of the 168 days with adequate data
coverage for diurnal analysis, 18.5% (31 days) displayed strong diurnal patterns: sixteen with elevated daytime emissions and
fifteen with elevated nocturnal emissions. Very few of these strong diurnal pattern days were contiguous: there were only four
instances of strong diurnal patterns persisting for two or more consecutive days. The periods with strong diurnal patterns when
395 F_{CH_4} peaked during the day were correlated with latent heat flux (Fig. S5, Fig. S6); while periods when F_{CH_4} peaked at night
were correlated with air pressure (Fig. S5, Fig. S6). While we looked for evidence of synoptic patterns in F_{CH_4} due to changes

in overlying pressure from frontal systems (c.f. Liu et al., 2016), and due to underwater turbulence (Fig. S7), we did not see evidence of impact on F_{CH_4} from these drivers during the study period.

3.2: Cumulative F_{CH_4}

400 There are notable differences in the cumulative annual areal emissions across methods and years (Table 1, Fig. 5). The impact of the spring burst is evident in the interannual difference between the EC cumulative emissions, which were 40.7 ± 5.88 and 71.4 ± 4.2 g CH_4 m^{-2} in 2017 and 2018, respectively. The cumulative areal emission measured by EC from 1 October 2017 through 1 May 2018 was 6.66 ± 3.1 g CH_4 m^{-2} , on the same order as the uncertainty range in the annual values. As follows from the patterns in the mean fluxes discussed above, the results from the spatial surveys and the shallow trap also indicate
405 elevated cumulative annual emissions in 2018 compared to 2017, while the results from the deep site indicate similar emissions over both years. The implications of the spring burst for whole-reservoir upscaled total annual CH_4 emissions is discussed below, but the best estimate of reservoir-wide cumulative annual areal emissions from the hybrid approach yields 45.6 ± 8.3 and 51.4 ± 4.3 g CH_4 m^{-2} for 2017 and 2018, respectively (Fig. 5). Scaling up to the 2.4 km^2 area of Acton Lake, the hybrid approach indicates that this reservoir was a source of 109 ± 14 and 122 ± 10 Mg CH_4 to the atmosphere in 2017 and 2018,
410 respectively.

3.3: Spatial patterns in F_{CH_4}

The results from the six spatial surveys indicate an inconsistent spatial pattern in F_{CH_4} that differs from previous findings on CH_4 emissions from temperate, eutrophic reservoirs which has shown that the river – reservoir transition zone near the tributary inlets tends to be a hot spot for emissions compared to the lacustrine zone (Beaulieu et al., 2014; Beaulieu et al., 2016; DeISontro
415 et al., 2011; Tuser et al., 2017). The survey results from Acton Lake indicate relatively similar rates of F_{CH_4} across most of the reservoir surface area (Fig. 6), and a weak but significant ($n=90$, $R^2 = 0.1$, $p < 0.005$) positive relationship between ebullition and reservoir depth (Fig. S8).

At the whole- reservoir scale, ebullition was a dominant emission pathway for CH_4 relative to diffusion, accounting for 82-94% of total F_{CH_4} . However, at certain sites diffusive F_{CH_4} contributed a larger proportion of the total flux (Fig. S9). The four
420 sites with mean ebullitive to total F_{CH_4} ratios less than 0.8 are also the four shallowest sites (see Fig. 1): U-09, U-14, U-07, and U-06, with mean observed depths of 1, 1.3, 1.5, and 2 m respectively. This pattern from the spatial surveys is also reflected in the results from the more frequent measurements made at the shallow and deep site: ebullition accounted for 58% of the total F_{CH_4} at the shallow site in both 2017 and 2018, while ebullition accounted for 86% and 88% of total F_{CH_4} at the deep site in 2017 and 2018, respectively. Emission behaviour at sites U-09 and U-06 was substantially different than at other sites: these
425 two sites had consistently low F_{CH_4} and tend to have higher rates of CH_4 diffusion than ebullition. Much of this behaviour is likely explained by the proximity of these sites to Acton Lake's swimming beach, which has a sandy substrate that likely inhibits methanogenesis at these sites. These sites were included as part of the random GRTS sampling design.

4. Discussion

4.1 Comparison with other systems and methods

430 The hybrid upscaling approach we used in this study leverages the best available information from our measurements to characterize both the spatial and temporal variability of Acton Lake: EC monitoring for the shallow portion of the reservoir, and the continuous deep site monitoring scaled by the spatial survey site measurements for the deep portion of the reservoir. If we used the EC monitoring results alone to upscale to whole-reservoir emissions, that would assume the spring burst pattern affected the whole reservoir (Fig. 5). However, we know the spring burst did not affect the deep site (Fig. 2). Thus, a key
435 uncertainty around this upscaling method is estimating what portion of the reservoir was affected by the spring burst of emissions in 2018. The cumulative F_{CH_4} measured by EC was 77% greater in 2018 than 2017, compared to a difference of only 11% per the hybrid approach. Adding one or more AFT sites along the depth gradient of the reservoir would be one way to decrease uncertainty in the extent of the spring burst and improve confidence in upscaled F_{CH_4} estimates.

Comparing cumulative annual areal emissions from the hybrid upscaling approach (45.6 ± 8.3 and 51.4 ± 4.3 g CH_4 m^{-2} for
440 2017 and 2018, respectively) to other reservoir CH_4 emission rates reported in the literature is not straightforward due to differences in monitoring methods and temporal coverage. One important reason earlier studies of reservoir F_{CH_4} may be biased low is that they only measured CH_4 diffusion: Deemer et al. (2016) found that the mean F_{CH_4} reported in studies measuring ebullition and diffusion was over double of diffusion-only F_{CH_4} studies. Another potentially important source of bias is temporal coverage. Most studies that report F_{CH_4} from inland waters monitor during the warm season, with less than six months of
445 measurements (cf. Deemer et al., 2016; DelSontro et al., 2018; Bastviken et al., 2011), and the mean F_{CH_4} value is then extrapolated to annual total emissions. However, we measured very low (on the same order as the warm-season uncertainty) wintertime F_{CH_4} in this study. On the other hand, the spring burst phenomenon we observed demonstrates the importance of continuous monitoring of mid-latitude eutrophic reservoirs during the full warm season to capture hot-moments of F_{CH_4} . A related consideration is a method's ability to capture spatial and temporal variability of F_{CH_4} during the study period. Deemer
450 et al. (2016) noted that studies using the eddy covariance method reported substantially higher values of F_{CH_4} : ~ 92.5 g CH_4 m^{-2} yr^{-1} (Deshmukh et al., 2014) and ~ 160 g CH_4 m^{-2} yr^{-1} (Eugster et al., 2011), which are on the same order as the Acton Lake cumulative annual emissions (Table 1). The two open-water sites included in the CH_4 EC meta-analysis by Knox et al., (2019) were natural lakes in temperate regions with cumulative annual emissions of ~ 15 g CH_4 m^{-2} yr^{-1} . This difference in F_{CH_4} speaks to the need for building a representative dataset across both methods and ecoregions.

455 Nevertheless, Acton Lake's annual F_{CH_4} is relatively high compared to other reservoirs. It falls in the 4th quintile (>60%) of the reservoir emission rates that included ebullition reported in Deemer et al., (2016); the warm season F_{CH_4} fall in the upper quintile (>80%) of those reservoirs. The warm season F_{CH_4} also falls into the upper quartile (>75%) of the 32 temperate reservoirs surveyed by Beaulieu et al. (2020). This result strengthens the finding that midlatitude, eutrophic reservoirs in the Midwest US can support high CH_4 emission rates (cf. Beaulieu et al., 2014, 2016) than would be predicted by age and latitude
460 alone (Barros et al., 2012). The high annual F_{CH_4} also supports the emerging body of knowledge around the importance of reservoir productivity as a key indicator for F_{CH_4} (cf. Deemer et al., 2016; West et al., 2012; DelSontro et al., 2018b).

4.2 Implications for upscaling

465 The key question in upscaling any set of measurements to characterize an ecosystem is “what is representative of reality?”. This study leveraged a combination of continuous and spatially extensive monitoring methods to investigate the spatial and temporal variability in a reservoir. The results from the six spatial surveys indicate an inconsistent spatial pattern in F_{CH_4} that differs from previous findings on CH_4 emissions from temperate, eutrophic reservoirs which has shown that the river – reservoir transition zone near the tributary inlets tends to be a hot spot for emissions compared to the lacustrine zone (Beaulieu et al., 470 2014; Beaulieu et al., 2016; DelSontro et al., 2011; Tuser et al., 2017). The spring burst of elevated emissions that we observed in 2018 but not 2017, and in the shallow portion of the reservoir but not at the deep site, is the largest contributor to the spatial and temporal variability in this study. In this section we will analyse the spring burst and factors that could have contributed to it. Other patterns in intra-reservoir spatial and temporal variability linked to sediment T and other biophysical drivers are also discussed.

475 4.2.1 Spring burst

Differences in phytoplankton populations and sediment temperature, partially driven by precipitation differences, provide insight into why the spring burst of emissions occurred 1) in 2018 but not 2017, and 2) in the littoral area of the reservoir but not the deeper areas. Chlorophyll a (chl_a) levels measured a few days before the spring burst period show elevated levels in the shallow portion of the reservoir in 2018 compared to 2017, while levels near the outflow were similar between the two years 480 (Fig. 7 (a)). This increase in chl_a levels coincided with an increase in shallow sed T to 27°C, (Fig. 7 (b)). These differences in chl_a and sedT near the inflow can be tied to differences in precipitation between the two years: spring of 2017 was relatively wet, with 31.0 cm of rainfall and 20.9×10^6 m³ of stream inflow in May (Fig. 4 (c), (d)) which drove substantial fluctuations in reservoir water level (Fig. 4 (e)). These rain events also led to a decrease in sedT from 22.5 to 18°C prior to the onset of the spring burst timeframe (Fig. 7 (b)) due to the inflow of cooler stream water and the cooling of ambient air temperature. In 485 contrast, May of 2018 was relatively dry, with 12.3 cm of rain, 9.45×10^6 m³ of stream inflow (Fig. 4 (c), (d)), and stable reservoir water levels (Fig. 4 (e)). The phytoplankton bloom in the shallow portion of the reservoir leading up to the spring burst period was likely catalyzed by the conducive water temperature, turbidity, and water level stability. Elevated levels of dissolved ammonium (NH₄), total phosphorus (TP), soluble reactive phosphorus (SRP), and particulate organic carbon (POC) near the inflow during the 2018 spring burst support that the conditions in the littoral area in 2018 were different than those in 490 2017, and that this interannual difference did not occur in the deep portion of the reservoir (Table 2).

There are at least two established mechanistic connections between phytoplankton blooms and enhanced CH_4 production and emission, and either or both could have driven the spring burst observed in this study. One mechanistic connection between autochthonous organic carbon (autoOC, i.e. phytoplankton-derived) and F_{CH_4} is the stimulation of methanogenesis from the input of this labile C source as the phytoplankton die and settle to the sediment. Several lab studies have demonstrated that the 495 addition of autoOC can lead to enhanced CH_4 production rates (Schwartz et al., 2008; West et al. 2012, 2015; Grasset et al., 2018). A recent study using in-situ measurements found that heatwave-induced cyanobacterial blooms and subsequent input of autoOC to the sediment could lead to pulses of CH_4 emissions up to an order of magnitude larger than baseline levels (Bartosiewicz et al., 2021). The 2018 crash in phytoplankton that coincided with the spring burst (as indicated by chl_a measurements, Fig. 7 (a)) evidences a large input of autoOC to the sediment during the spring burst. A second possible

500 mechanistic connection is production of CH₄ by phytoplankton in the oxic surface water. A recent study by Hartmann et al. (2020) combined in-situ measurements of phytoplankton communities, CH₄, and CH₄ isotopes with lab incubations and demonstrated that all major phytoplankton classes could produce CH₄ under oxic conditions. Phytoplankton CH₄ production in the surface mixed layer super-saturates the upper water column with CH₄ and leads to enhanced diffusive emissions, and phytoplankton biomass has been found to be the primary driver of diffusive F_{CH₄} in some reservoir systems (McClure et al., 505 2020). Strong diurnal patterns in F_{CH₄} surrounding the spring burst correlated with latent heat flux (LE), an indicator of warm, windy, convective conditions of enhanced air-water gas exchange (Fig. S5, S6). This suggests that during the spring burst the surface waters were super-saturated with CH₄ and diffusive emissions were the dominant pathway during that time. Including measures of phytoplankton CH₄ production in the surface mixed layer in future studies would be helpful in differentiating which production pathway led to elevated dissolved CH₄.

510 The difference in hydrologic regimes and subsequent availability of autoOC versus allochthonous OC (alloOC, i.e. particulate or dissolved C derived from terrestrial plant tissue) may also shed light on interannual differences beyond the spring burst. The lab study by Grasset et al. (2018) found that while additions of autoOC led to pulses of F_{CH₄}, alloOC took longer to decompose and additions led to more gradual but sustained F_{CH₄}. Thus, the wet spring of 2017 may have loaded the reservoir with slow-burning alloOC, which could partially explain the smaller magnitude of F_{CH₄} pulses in 2017 compared to 2018 (Fig. 2).

515 The impact, or lack thereof, of the spring burst on reservoir-wide cumulative F_{CH₄} has implications for the value of higher-resolution measurements. This is analogous to the question of whether the increased complexity of process-based models improves prediction over empirical models (cf. Adams et al., 2013). While the EC monitoring results almost doubled from 2017 to 2018, the hybrid upscaled estimate had only an 11% difference (Table 1, Fig. 5). Furthermore, the cumulative F_{CH₄} determined via the lake-wide surveys was closer to the hybrid upscaled estimate than the EC results in 2018 (Fig. 5). Using the recent size-productivity model (Del Sontro et al., 2018) to predict F_{CH₄} at Acton Lake based on mean annual chl_a levels (Eq. 7, 520 Fig 7) yields estimates of 11.1 and 10.3 mg CH₄ m⁻² hr⁻¹ for 2017 and 2018, respectively. These values are in the same range as the warm season mean fluxes determined via the hybrid approach for Acton Lake (Table 1). However, the model results contrast with measured results in terms of which year had higher F_{CH₄}. Furthermore, the model results would over-estimate cumulative annual F_{CH₄} for Acton Lake as they do not take low wintertime emissions into account.

525 Sub-annual climatic patterns and productivity dynamics may become more important in understanding and predicting reservoir F_{CH₄}. Recent research demonstrates how warmer springs have increased the frequency and intensity of cyanobacterial blooms in midwestern US reservoirs over the past two decades (Smucker et al., 2021), and continued warming will likely intensify this phenomenon. There is also a burgeoning body of knowledge that points to the importance of phytoplankton ecology on lake and reservoir CH₄ production, in terms of both the amount (Hartman et al., 2020; McClure et al., 2020; Zhang et al., 2021) and 530 type (Bartosiewicz et al., 2021). Furthermore, Thus, the underlying factors that led to the 2018 spring burst at Acton Lake may be more common in the future and have a greater effect on the reservoir CH₄ budget.

4.2.2 Additional intra-lake variability:

Beyond the spring burst, we observed additional patterns of intra-lake spatiotemporal variability in F_{CH₄} related to sediment 535 temperature (sedT). Temperature is an important control on metabolic processes such as methanogenesis, but other signals can

complicate the relationship between temperature and F_{CH_4} at the scale of ecosystem fluxes. Nevertheless, sedT emerged as a key predictor of F_{CH_4} in this study. The ANN model used to gap-fill the EC monitoring ranked sedT as one of the most important biophysical predictors of F_{CH_4} along with absolute static pressure, change in static pressure, and latent heat flux (Fig. 3). A strong indication of the intra-lake patterns in drivers and emissions is that maximum ebullitive F_{CH_4} observed by the AFTs coincided with maximum sedT at both the shallow (U-14) and deep (U-12) monitoring sites in 2017 (Fig. 8). This maximum occurs in early August at U-14 versus mid-September at U-12, a phase-shift that reflects the time delay in heat transfer to the deeper sediment. This phase shift could also (speculatively) have been affected by the time delay in nutrient and OC transfer from the inlets. This pattern was not as pronounced in 2018 (Fig. S10), perhaps due to differences in the precipitation regime that affected reservoir metabolism.

We used ecoQ10 and 2DKS threshold analysis to further investigate the role of sediment temperature on regulating F_{CH_4} in both the deep and shallow portions of Acton Lake. Both of these quantitative analyses of the relationship between F_{CH_4} and SedT yielded statistically significant results (Table 3), and each monitoring method had consistent ecoQ10 values and 2DKS threshold temperatures across the two study years (Table 3, Fig S11). The EC method had a much lower ecoQ10 value than the AFT sites, the latter of which were comparable to maximum ecoQ10 values reported in other studies (DelSontro et al., 2016). The relatively low ecoQ10 value for the EC method may be due to different T response of ebullitive vs. diffusive emission pathways, or to a spatial mis-match between the measured sedT and the EC flux footprint. For these reasons, we focus on the AFT sites in interpreting the ecoQ10 and threshold temperature results in terms of intra-lake spatial variability. The ecoQ10 values indicate a stronger relationship between sedT and ebullitive F_{CH_4} at the shallow site than the deep site. Despite a greater ecoQ10 value, ebullitive F_{CH_4} at the shallow site didn't respond to warming in the spring until water temperatures reached a threshold of ~22.5 °C, whereas ebullitive F_{CH_4} at the deep site responded to warming at a much lower temperature threshold (13 – 18 °C, Table 3). Furthermore, mean ebullitive F_{CH_4} was very similar between the two sites (Table 1), despite a 6-degree difference in maximum sediment temperature. These patterns suggest that methanogens at the deep site may be better adapted to the consistently cooler conditions found in the hypolimnion of Acton Lake, which has important implications for predictive models employing ecoQ10 or threshold values to parameterize F_{CH_4} as a function of sedT. Alternatively, the differences in temperature sensitivity between the deep and shallow site may reflect differences in substrate quality and/or quantity related to spatial patterns in sedimentation and productivity (Berberich et al. 2019). Regardless of the underlying mechanism, these patterns illustrate strong spatial patterning in CH_4 biogeochemistry within this 2.4 km² reservoir.

5. Conclusions

In this study we investigated temporal patterns and biophysical drivers of CH_4 fluxes from a eutrophic temperate reservoir using multiple methods including eddy covariance. Sediment temperature and the overlying static pressure were the most important biophysical drivers of F_{CH_4} per the ANN model results. Water chemistry and chl_a measurements indicate that the spring burst of elevated F_{CH_4} coincided with a phytoplankton bloom. Comparing the two observation years indicated that the climatic conditions of precipitation and temperature were more conducive to a phytoplankton bloom in 2018 than 2017. In contrast to previous studies, we saw a weak positive correlation between F_{CH_4} and reservoir depth, we did not find a strong relationship between F_{CH_4} and underwater turbulence, nor did we observe consistent diurnal patterns in F_{CH_4} .

We found that Acton Lake had cumulative annual CH₄ areal emissions of 45.6 ± 8.3 and 51.4 ± 4.3 g CH₄ m⁻² in 2017 and 2018, respectively. These levels of emissions place Acton Lake in the upper quartile of emission rates reported from reservoirs (Deemer et al., 2016), further supporting the concept that highly productive mid-latitude reservoirs can have higher magnitude CH₄ emission rates than would be predicted by age and latitude alone (Del Sontro et al., 2018). A spring burst of F_{CH₄} observed
575 over a two-week period in 2018 but not 2017 accounted for 59% of the difference in cumulative emissions between years. This difference between consecutive years highlights the importance of multi-year studies (c.f. Room et al., 2014), and the importance of characterizing temporal variability in open water systems, which Williamson et al. (2020) illustrated exceeded spatial variability for several physical, chemical, and biological metrics.

The EC technique holds much promise for improving our understanding of the biophysical drivers of gaseous fluxes, with a
580 few caveats. In addition to the pseudo-continuous temporal coverage, the EC measurement footprint encompasses a much larger area than traditional gas flux measurement techniques (e.g. dissolved gas sampling, chambers, inverted funnel traps), increasing the likelihood of integrating fluxes over a distribution of hot spots. However, care must be taken in the siting, quality control, and interpretation of results. The authors reemphasize the recommendation given by Vesala et al., (2012): for best results, close collaboration is needed between biometeorologists and limnologists, to understand what is going on both above
585 and below the water. For future studies of reservoir F_{CH₄} using EC, we recommend siting the monitoring tower in the area of the reservoir with the highest variability in CH₄ emissions, likely near the inlet, and setting up multiple AFTs across the reach of the reservoir to constrain spatial patterns. Future studies that incorporate more direct measurements of phytoplankton dynamics would also be useful to improve our understanding of drivers of CH₄ production and emission that may be more common with future warmer springs and extremes in precipitation patterns.

590 The EC results in this study further our understanding of the interaction between precipitation, sediment temperature, algal productivity levels, and F_{CH₄}. This study adds to our understanding of open water flux processes at appropriate spatial and temporal scales, while highlighting a way to present and compare EC and whole- reservoir survey data in appropriate contexts.

Code and Data Availability

595 The datasets and R code used for the analysis in this study are available on Zenodo. The raw data and R code are available under: R Code for: Temporal patterns and biophysical controls on methane emissions from a small eutrophic reservoir: insights from two years of eddy covariance monitoring, doi: 10.5281/zenodo.4540271; and supplemental ANN resampling data is available under: Artificial Neural Network (ANN) Resampling Results for Gap Filling Eddy Covariance Data, doi: 10.5281/zenodo.4540271.

600 Author Contributions

1. S. Waldo: conceptualization, data curation, formal analysis, investigation, methodology, project administration, software, visualization, writing – original draft, writing – review & editing

2. J.J. Beaulieu: conceptualization, data curation, formal analysis, funding acquisition, investigation, methodology, project administration, resources, software, supervision, writing – review & editing
- 605 3. W. Barnett: formal analysis, methodology, software, writing – review & editing
4. D.A. Balz: conceptualization, data curation, investigation, methodology, project administration, resources, supervision
5. M.J. Vanni: data curation, formal analysis, investigation, resources, writing – review & editing
6. T. Williamson: data curation, formal analysis, investigation, resources
7. J.T. Walker: conceptualization, funding acquisition, investigation, methodology, project administration, resources,
610 supervision, writing – review & editing

Disclaimer

The views expressed in this article are those of the authors and do not necessarily reflect the views and policies of the US Environmental Protection Agency. Any mention of trade names, manufacturers or products does not imply an endorsement by the United States Government or the US Environmental Protection Agency. EPA and its employees do not endorse any commercial products, services, or enterprises.

615

Acknowledgements

We thank David Wesler and other personnel at Hueston Wood State Park for all of their support in our monitoring efforts at Acton Lake. We are very grateful to the members of the EPA Scientific Dive Unit for their assistance in installing the mid-lake tower: Steve Donahue, Brad White, Frank Borsuk, David Light, Nathan Doyle, and Leah Ettema. We also thank Gil Bohrer and Jorge Villa for their guidance and assistance with the mid-lake tower. We thank Ryan Daly, Bill Mitchell, and Garrett Wiley for assistance with design and fabrication of tower hardware and power systems. We are grateful for the additional laboratory and field support provided by Karen White, Paul Trygstad, Eleanor Silver, Megan Berberich, Keith Bisbe, Aiden Pemberton, Page Jordan, and Tom Radford. We would also like to thank the three anonymous referees who provided valuable constructive feedback that improved the quality of this paper. We acknowledge that Acton Lake is located within the traditional homelands of the Myaamia and Shawnee people, who along with other indigenous groups ceded these lands to the United States in the first Treaty of Greenville in 1795.

620

625

References

- 630 Adams, H., Williams, A., Xu, C., Rauscher, S, Jiang, X., and McDowell, N. (2013). Empirical and process-based approaches to climate-induced forest mortality models. *Frontiers in Plant Science*. <https://doi.org/10.3389/fpls.2013.00438>
- Andersen, I. M., Williamson, T. J., González, M. J., & Vanni, M. J. (2020). Nitrate, ammonium, and phosphorus drive seasonal nutrient limitation of chlorophytes, cyanobacteria, and diatoms in a hyper-eutrophic reservoir. *Limnology and Oceanography*, *65*(5), 962–978. <https://doi.org/10.1002/lno.11363>
- 635 Aubinet, M., Feigenwinter, C., Heinesch, B., Laffineur, Q., Papale, D., Reichstein, M., ... Van Gorsel, E. (2012). Nighttime Flux Correction. In M. Aubinet, T. Vesala, & D. Papale (Eds.), *Eddy Covariance* (pp. 133–157). Dordrecht: Springer Netherlands. https://doi.org/10.1007/978-94-007-2351-1_5
- Barros, N., Cole, J.J., Tranvik, L.J., Prairie, Y.T., Bastviken, D., Huszar, V.L., Del Giorgio, P. and Roland, F., 2011. Carbon emission from hydroelectric reservoirs linked to reservoir age and latitude. *Nature Geoscience*, *4*(9), pp.593-596.
- 640 Barnett, Will, Waldo, Sarah, & Beaulieu, Jake. (2021, February 13). R Code for: Temporal patterns and biophysical controls on methane emissions from a small eutrophic reservoir: insights from two years of eddy covariance monitoring. Zenodo. <http://doi.org/10.5281/zenodo.4540271>
- Bartosiewicz, Maciej , Roxane Maranger, Anna Przytulska, Isabelle Laurion, Effects of phytoplankton blooms on fluxes and emissions of greenhouse gases in a eutrophic lake, *Water Research* (2021).
- 645 Bastien, J. (2011). CO₂ and CH₄ diffusive and degassing fluxes from 2003 to 2009 at Eastmain 1 reservoir, Québec, Canada. *Inland Waters*, *1*(2), 113–123. <https://doi.org/10.5268/IW-1.2.349>
- Bastviken, D., Tranvik, L. J., Downing, J. A., Crill, P. M., & Enrich-Prast, A. (2011). Freshwater methane emissions offset the continental carbon sink. *Science*, *331*(6013), 50–50. <https://doi.org/10.1126/science.1196808>
- Beaulieu, J. J., Balz, D. A., Birchfield, M. K., Harrison, J. A., Nietch, C. T., Platz, M. C., ... Young, J. L. (2018). Effects of an experimental water-level drawdown on methane emissions from a eutrophic reservoir. *Ecosystems*, *21*(4), 657–674. <https://doi.org/10.1007/s10021-017-0176-2>
- 650 Beaulieu, J. J., McManus, M. G., & Nietch, C. T. (2016). Estimates of reservoir methane emissions based on a spatially balanced probabilistic-survey: Reservoir Methane Emissions. *Limnology and Oceanography*, *61*(S1), S27–S40. <https://doi.org/10.1002/lno.10284>

- 655 Beaulieu, J. J., Smolenski, R. L., Nietch, C. T., Townsend-Small, A., & Elovitz, M. S. (2014). High methane emissions from a midlatitude reservoir draining an agricultural watershed. *Environmental Science & Technology*, 48(19), 11100–11108. <https://doi.org/10.1021/es501871g>
- Beaulieu, J.J., Balz, D.A., Birchfield, M.K., Harrison, J.A., Nietch, C.T., Platz, M.C., Squier, W.C., Waldo, S., Walker, J.T., White, K.M. and Young, J.L., 2018. Effects of an experimental water-level drawdown on methane emissions from a eutrophic reservoir. *Ecosystems*, 21(4), pp.657-674.
- 660 Beaulieu, J.J., Waldo, S., Balz, D.A., Barnett, W., Hall, A., Platz, M.C. and White, K.M., 2020. Methane and carbon dioxide emissions from reservoirs: controls and upscaling. *Journal of Geophysical Research: Biogeosciences*, 125(12), p.e2019JG005474.
- Berberich, M. E., Beaulieu, J. J., Hamilton, T. L., Waldo, S., & Buffam, I. (2019). Spatial variability of sediment methane production and methanogen communities within a eutrophic reservoir: Importance of organic matter source and quantity. *Limnology and Oceanography*, n/a(n/a). <https://doi.org/10.1002/lno.11392>
- 665 Cole, J. J., Prairie, Y. T., Caraco, N. F., McDowell, W. H., Tranvik, L. J., Striegl, R. G., ... Melack, J. (2007). Plumbing the global carbon cycle: integrating inland waters into the terrestrial carbon budget. *Ecosystems*, 10(1), 172–185. <https://doi.org/10.1007/s10021-006-9013-8>
- 670 Deemer, B. R., Harrison, J. A., Li, S., Beaulieu, J. J., DelSontro, T., Barros, N., ... Vonk, J. A. (2016). Greenhouse gas emissions from reservoir water surfaces: A new global synthesis. *BioScience*, 66(11), 949–964. <https://doi.org/10.1093/biosci/biw117>
- DelSontro, T., Boutet, L., St-Pierre, A., del Giorgio, P. A., & Prairie, Y. T. (2016). Methane ebullition and diffusion from northern ponds and lakes regulated by the interaction between temperature and system productivity: Productivity regulates methane lake flux. *Limnology and Oceanography*, 61(S1), S62–S77. <https://doi.org/10.1002/lno.10335>
- 675 DelSontro, T., Kunz, M. J., Kempter, T., Wüest, A., Wehrli, B., & Senn, D. B. (2011). Spatial heterogeneity of methane ebullition in a large tropical reservoir. *Environmental Science & Technology*, 45(23), 9866–9873. <https://doi.org/10.1021/es2005545>
- DelSontro, T., Giorgio, P., Prairie, Y. (2018a). No longer a paradox: the interaction between physical transport and biological processes explains the spatial distribution of surface water methane within and across lakes. *Ecosystems*. 21. [10.1007/s10021-017-0205-1](https://doi.org/10.1007/s10021-017-0205-1).
- 680

- DelSontro, T., Beaulieu, J., Downing, J. (2018b). Greenhouse gas emissions from lakes and impoundments: Upscaling in the face of global change. *Limnology and Oceanography Letters*, 3. 10.1002/lol2.10073.
- Demarty, M., Bastien, J., & Tremblay, A. (2011). Annual follow-up of gross diffusive carbon dioxide and methane emissions from a boreal reservoir and two nearby lakes in Québec, Canada. *Biogeosciences*, 8(1), 41–53.
685 <https://doi.org/10.5194/bg-8-41-2011>
- Dengel, S., Zona, D., Sachs, T., Aurela, M., Jammet, M., Parmentier, F. J. W., ... Vesala, T. (2013). Testing the applicability of neural networks as a gap-filling method using CH₄ flux data from high latitude wetlands. *Biogeosciences*, 10(12), 8185–8200. <https://doi.org/10.5194/bg-10-8185-2013>
- Deshmukh, C., Serça, D., Delon, C., Tardif, R., Demarty, M., Jarnot, C., ... Guérin, F. (2014). Physical controls on CH₄ emissions from a newly flooded subtropical freshwater hydroelectric reservoir: Nam Theun 2. *Biogeosciences*, 11(15), 4251–4269. <https://doi.org/10.5194/bg-11-4251-2014>
- Duc, N. T., Crill, P., & Bastviken, D. (2010). Implications of temperature and sediment characteristics on methane formation and oxidation in lake sediments. *Biogeochemistry*, 100(1–3), 185–196. <https://doi.org/10.1007/s10533-010-9415-8>
- Eugster, W., DelSontro, T., & Sobek, S. (2011). Eddy covariance flux measurements confirm extreme CH₄ emissions from a Swiss hydropower reservoir and resolve their short-term variability. *Biogeosciences*, 8(9), 2815–2831.
695 <https://doi.org/10.5194/bg-8-2815-2011>
- Finkelstein, P. L., & Sims, P. F. (2001). Sampling error in eddy correlation flux measurements. *Journal of Geophysical Research: Atmospheres*, 106(D4), 3503–3509. <https://doi.org/10.1029/2000JD900731>
- Foken, T. M., Gockede, M., Mauder, L., Mahrt, L., Amiro, B. D., & Munger, J. W. (2004). Post-field quality control. In *Handbook of micrometeorology: a guide for surface flux measurements*. Dordrecht: Kluwer Academic.
- Fuchs, A., Lyautey, E., Montuelle, B., & Casper, P. (2016). Effects of increasing temperatures on methane concentrations and methanogenesis during experimental incubation of sediments from oligotrophic and mesotrophic lakes: Temperature Effects on CH₄. *Journal of Geophysical Research: Biogeosciences*, 121(5), 1394–1406.
705 <https://doi.org/10.1002/2016JG003328>
- Garvey, J. E., Marschall, E. A., & Wright, R. A. (1998). from star charts to stoneflies: detecting relationships in continuous bivariate data. *Ecology*, 79(2), 442–447. [https://doi.org/10.1890/0012-9658\(1998\)079\[0442:FSCTSD\]2.0.CO;2](https://doi.org/10.1890/0012-9658(1998)079[0442:FSCTSD]2.0.CO;2)
- Grasset, C., Mendonça, R., Villamor Saucedo, G., Bastviken, D., Roland, F., & Sobek, S. (2018). Large but variable methane production in anoxic freshwater sediment upon addition of allochthonous and autochthonous organic matter:

- 710 Methanogenic potential of different OC types. *Limnology and Oceanography*, 63(4), 1488–1501.
<https://doi.org/10.1002/lno.10786>
- Harrison, J. A., Deemer, B. R., Birchfield, M. K., & O'Malley, M. T. (2017). Reservoir water-level drawdowns accelerate and amplify methane emission. *Environmental Science & Technology*, 51(3), 1267–1277.
<https://doi.org/10.1021/acs.est.6b03185>
- 715 Hartmann, J. F., M. Gunthel, T. Klintzsch, G. Kirillin, H. P. Grossart, F. Keppler, and M. Isenbeck-Schroter. 2020. High spatiotemporal dynamics of methane production and emission in oxic surface water. *Environmental Science & Technology* 54:1451-1463.
- Hayes, N. M., Deemer, B. R., Corman, J. R., Razavi, N. R., & Strock, K. E. (2017). Key differences between lakes and reservoirs modify climate signals: A case for a new conceptual model. *Limnology and Oceanography Letters*, 2(2),
720 47–62. <https://doi.org/10.1002/lol2.10036>
- Higgins, C. W., Pardyjak, E., Froidevaux, M., Simeonov, V., & Parlange, M. B. (2013). Measured and estimated water vapor advection in the atmospheric surface layer. *Journal of Hydrometeorology*, 14(6), 1966–1972.
<https://doi.org/10.1175/JHM-D-12-0166.1>
- Jammet, M., Crill, P., Dengel, S., & Friborg, T. (2015). Large methane emissions from a subarctic lake during spring thaw: Mechanisms and landscape significance. *Journal of Geophysical Research: Biogeosciences*, 120(11), 2289–2305.
725 <https://doi.org/10.1002/2015JG003137>
- Jammet, M., Dengel, S., Kettner, E., Parmentier, F.-J. W., Wik, M., Crill, P., & Friborg, T. (2017). Year-round CH₄ and CO₂ flux dynamics in two contrasting freshwater ecosystems of the subarctic. *Biogeosciences*, 14(22), 5189–5216.
<https://doi.org/10.5194/bg-14-5189-2017>
- 730 Juutinen, S., Rantakari, M., Kortelainen, P., Huttunen, J. T., Larmola, T., Alm, J., ... Martikainen, P. J. (2009). Methane dynamics in different boreal lake types. *Biogeosciences*, 6(2), 209–223. <https://doi.org/10.5194/bg-6-209-2009>
- Kenny, W. T., Bohrer, G., Morin, T. H., Vogel, C. S., Matheny, A. M., & Desai, A. R. (2017). A numerical case study of the implications of secondary circulations to the interpretation of eddy-covariance measurements over small lakes. *Boundary-Layer Meteorology*, 165(2), 311–332. <https://doi.org/10.1007/s10546-017-0268-8>
- 735 Kincaid, T., Olsen, A., & Weber, M. (2019). spsurvey: Spatial survey design and analysis (Version 4.1.0) [R package].

- Kljun, N., Calanca, P., Rotach, M. W., & Schmid, H. P. (2015). A simple two-dimensional parameterisation for Flux Footprint Prediction (FFP). *Geoscientific Model Development*, 8(11), 3695–3713. <https://doi.org/10.5194/gmd-8-3695-2015>
- 740 Knoll, L. B., Vanni, M. J., Renwick, W. H., Dittman, E. K., & Gephart, J. A. (2013). Temperate reservoirs are large carbon sinks and small CO₂ sources: Results from high-resolution carbon budgets. *Global Biogeochemical Cycles*, 27(1), 52–64. <https://doi.org/10.1002/gbc.20020>
- Knox, Sara H., Jackson, R. B., Poulter, B., McNicol, G., Fluet-Chouinard, E., Zhang, Z., ... Zona, D. (2019). FLUXNET-CH₄ Synthesis Activity: Objectives, Observations, and Future Directions. *Bulletin of the American Meteorological Society*, 100(12), 2607–2632. <https://doi.org/10.1175/BAMS-D-18-0268.1>
- 745 Knox, Sara Helen, Matthes, J. H., Sturtevant, C., Oikawa, P. Y., Verfaillie, J., & Baldocchi, D. (2016). Biophysical controls on interannual variability in ecosystem-scale CO₂ and CH₄ exchange in a California rice paddy. *Journal of Geophysical Research: Biogeosciences*, 121(3), 978–1001. <https://doi.org/10.1002/2015JG003247>
- Knox, Sara Helen, Sturtevant, C., Matthes, J. H., Koteen, L., Verfaillie, J., & Baldocchi, D. (2015). Agricultural peatland restoration: effects of land-use change on greenhouse gas (CO₂ and CH₄) fluxes in the Sacramento-San Joaquin Delta. *Global Change Biology*, 21(2), 750–765. <https://doi.org/10.1111/gcb.12745>
- 750 Liu, H., Zhang, Q., & Dowler, G. (2012). Environmental controls on the surface energy budget over a large southern inland water in the united states: an analysis of one-year eddy covariance flux data. *Journal of Hydrometeorology*, 13(6), 1893–1910. <https://doi.org/10.1175/JHM-D-12-020.1>
- Liu, H., Zhang, Q., Katul, G. G., Cole, J. J., Chapin, F. S., & MacIntyre, S. (2016). Large CO₂ effluxes at night and during synoptic weather events significantly contribute to CO₂ emissions from a reservoir. *Environmental Research Letters*, 11(6), 064001. <https://doi.org/10.1088/1748-9326/11/6/064001>
- 755 Lofton, D. D., Whalen, S. C., & Hershey, A. E. (2014). Effect of temperature on methane dynamics and evaluation of methane oxidation kinetics in shallow Arctic Alaskan lakes. *Hydrobiologia*, 721(1), 209–222. <https://doi.org/10.1007/s10750-013-1663-x>
- 760 Lopes, R. H. C., Hobson, P. R., & Reid, I. D. (2008). Computationally efficient algorithms for the two-dimensional Kolmogorov–Smirnov test. *Journal of Physics: Conference Series*, 119(4), 042019. <https://doi.org/10.1088/1742-6596/119/4/042019>

- Lovelock, C. E., Evans, C., Barros, N., Prairie, Y. T., Alm, J., Bastviken, D., ... Stepanenko, V. (2019). 2019 Refinement to the 2006 IPCC Guidelines for National Greenhouse Gas Inventories: IPCC, chap. 7, v. 4, p. 7.1-7.54. Retrieved from
765 <https://www.ipcc-nggip.iges.or.jp/public/2019rf/index.html>
- Maeck, A., DelSontro, T., McGinnis, D. F., Fischer, H., Flury, S., Schmidt, M., ... Lorke, A. (2013). Sediment trapping by dams creates methane emission hot spots. *Environmental Science & Technology*, 47(15), 8130–8137.
<https://doi.org/10.1021/es4003907>
- Martinet, J., Guédant, P., & Descloux, S. (2016). Phytoplankton community and trophic status assessment of a newly
770 impounded sub-tropical reservoir: case study of the Nam Theun 2 Reservoir (Lao PDR, Southeast Asia).
Hydroécologie Appliquée, 19, 173–195. <https://doi.org/10.1051/hydro/2015006>
- McClure, R.P., M. E. Lofton, S. Chen, K. M. Krueger, J. C. Little, C. C. Carey, The magnitude and drivers of methane ebullition and diffusion vary on a longitudinal gradient in a small freshwater reservoir, *Journal of Geophysical Research: Biogeosciences*, 10.1029/2019JG005205, 125, 3, (2020).
- 775 McDermitt, D., Burba, G., Xu, L., Anderson, T., Komissarov, A., Riensche, B., ... Hastings, S. (2011). A new low-power, open-path instrument for measuring methane flux by eddy covariance. *Applied Physics B*, 102(2), 391–405.
<https://doi.org/10.1007/s00340-010-4307-0>
- Moffat, A. M., Papale, D., Reichstein, M., Hollinger, D. Y., Richardson, A. D., Barr, A. G., ... Stauch, V. J. (2007). Comprehensive comparison of gap-filling techniques for eddy covariance net carbon fluxes. *Agricultural and Forest
780 Meteorology*, 147(3–4), 209–232. <https://doi.org/10.1016/j.agrformet.2007.08.011>
- Moncrieff, J. B., Clement, R., Finnigan, J., & Meyers, T. (2004). Averaging, detrending and filtering of eddy covariance time series. In X. Lee, W. J. Massman, & B. E. Law (Eds.), *Handbook of Micrometeorology: a guide for surface flux measurements* (pp. 7–31). Dordrecht: Kluwer Academic.
- Moncrieff, J. B., Malhi, Y., & Leuning, R. (1996). The propagation of errors in long-term measurements of land-atmosphere
785 fluxes of carbon and water. *Global Change Biology*, 2(3), 231–240. <https://doi.org/10.1111/j.1365-2486.1996.tb00075.x>
- Moncrieff, J. B., Massheder, J. M., de Bruin, H., Elbers, J., Friborg, T., Heusinkveld, B., ... Verhoef, A. (1997). A system to measure surface fluxes of momentum, sensible heat, water vapour and carbon dioxide. *Journal of Hydrology*, 188–189, 589–611. [https://doi.org/10.1016/S0022-1694\(96\)03194-0](https://doi.org/10.1016/S0022-1694(96)03194-0)

- 790 Morin, T. H., Bohrer, G., Frasson, R. P. d. M., Naor-Azreli, L., Mesi, S., Stefanik, K. C., & Schäfer, K. V. R. (2014). Environmental drivers of methane fluxes from an urban temperate wetland park. *Journal of Geophysical Research: Biogeosciences*, *119*(11), 2188–2208. <https://doi.org/10.1002/2014JG002750>
- Nemitz, E., Mammarella, I., Ibrom, A., Aurela, M., Burba, G. G., Dengel, S., ... Zahniser, M. (2018). Standardisation of eddy-covariance flux measurements of methane and nitrous oxide. *International Agrophysics*, *32*(4), 517–549. <https://doi.org/10.1515/intag-2017-0042>
- 795 Olsen, A. R., Kincaid, T. M., & Payton, Q. (2012). Spatially balanced survey designs for natural resources. In R. A. Gitzen, J. J. Millspaugh, A. B. Cooper, & D. S. Licht (Eds.), *Design and Analysis of Long-term Ecological Monitoring Studies* (pp. 126–150). Cambridge: Cambridge University Press. <https://doi.org/10.1017/CBO9781139022422.010>
- Podgrajsek, E., Sahlée, E., Bastviken, D., Holst, J., Lindroth, A., Tranvik, L., & Rutgersson, A. (2014). Comparison of floating chamber and eddy covariance measurements of lake greenhouse gas fluxes. *Biogeosciences*, *11*(15), 4225–4233. <https://doi.org/10.5194/bg-11-4225-2014>
- 800 Podgrajsek, E., Sahlée, E., & Rutgersson, A. (2014). Diurnal cycle of lake methane flux: Diurnal cycle of lake methane flux. *Journal of Geophysical Research: Biogeosciences*, *119*(3), 236–248. <https://doi.org/10.1002/2013JG002327>
- Renwick, W. H., Vanni, M. J., Fisher, T. J., & Morris, E. L. (2018). Stream nitrogen, phosphorus, and sediment concentrations show contrasting long-term trends associated with agricultural change. *Journal of Environmental Quality*, *47*(6), 1513–1521. <https://doi.org/10.2134/jeq2018.04.0162>
- 805 Rey-Sanchez, A. C., Morin, T. H., Stefanik, K. C., Wrighton, K., & Bohrer, G. (2018). Determining total emissions and environmental drivers of methane flux in a Lake Erie estuarine marsh. *Ecological Engineering*, *114*, 7–15. <https://doi.org/10.1016/j.ecoleng.2017.06.042>
- 810 Richardson, A. D., Hollinger, D. Y., Burba, G. G., Davis, K. J., Flanagan, L. B., Katul, G. G., ... Wofsy, S. C. (2006). A multi-site analysis of random error in tower-based measurements of carbon and energy fluxes. *Agricultural and Forest Meteorology*, *136*(1–2), 1–18. <https://doi.org/10.1016/j.agrformet.2006.01.007>
- Ripley, B., & Venables, W. (2020). nnet: Feed-Forward Neural Networks and Multinomial Log-Linear Models (Version 7.3-13). Retrieved from <https://CRAN.R-project.org/package=nnet>
- 815 Rõõm, E.-I., Nõges, P., Feldmann, T., Tuvikene, L., Kisand, A., Teearu, H., & Nõges, T. (2014). Years are not brothers: Two-year comparison of greenhouse gas fluxes in large shallow Lake Võrtsjärv, Estonia. *Journal of Hydrology*, *519*, 1594–1606. <https://doi.org/10.1016/j.jhydrol.2014.09.011>

- Sahlée, E., Rutgersson, A., Podgrajsek, E., & Bergström, H. (2014). Influence from surrounding land on the turbulence measurements above a lake. *Boundary-Layer Meteorology*, *150*(2), 235–258. <https://doi.org/10.1007/s10546-013-9868-0>
- 820
- Schubert, C. J., Diem, T., & Eugster, W. (2012). Methane emissions from a small wind shielded lake determined by eddy covariance, flux chambers, anchored funnels, and boundary model calculations: a comparison. *Environmental Science & Technology*, *46*(8), 4515–4522. <https://doi.org/10.1021/es203465x>
- Schwarz, J. I. K., Eckert, W., & Conrad, R. (2008). Response of the methanogenic microbial community of a profundal lake sediment (Lake Kinneret, Israel) to algal deposition. *Limnology and Oceanography*, *53*(1), 113–121. <https://doi.org/10.4319/lo.2008.53.1.0113>
- 825
- Segers, R. (1998). Methane production and methane consumption: a review of processes underlying wetland methane fluxes. *Biogeochemistry*, *41*(1), 23–51. <https://doi.org/10.1023/A:1005929032764>
- Smucker, N.J., Beaulieu, J.J., Nietch, C.T. and Young, J.L., 2021. Increasingly severe cyanobacterial blooms and deep water hypoxia coincide with warming water temperatures in reservoirs. *Global Change Biology*, *27*(11), pp.2507-2519.
- 830
- Stevens, D. L., & Olsen, A. R. (2003). Variance estimation for spatially balanced samples of environmental resources. *Environmetrics*, *14*(6), 593–610. <https://doi.org/10.1002/env.606>
- Thornton, K. W., Kimmel, B. L., & Payne, F. E. (Eds.). (1990). *Reservoir limnology: ecological perspectives*. New York: Wiley.
- 835
- Tušer, M., Píček, T., Sajdlová, Z., Jůza, T., Muška, M., & Frouzová, J. (2017). Seasonal and spatial dynamics of gas ebullition in a temperate water-storage reservoir. *Water Resources Research*, *53*(10), 8266–8276. <https://doi.org/10.1002/2017WR020694>
- Varadharajan, C., & Hemond, H. F. (2012). Time-series analysis of high-resolution ebullition fluxes from a stratified, freshwater lake. *Journal of Geophysical Research: Biogeosciences*, *117*(G2), n/a-n/a.
- 840
- <https://doi.org/10.1029/2011JG001866>
- Varadharajan, C., Hermosillo, R., & Hemond, H. F. (2010). A low-cost automated trap to measure bubbling gas fluxes. *Limnology and Oceanography: Methods*, *8*(7), 363–375. <https://doi.org/10.4319/lom.2010.8.363>
- Vesala, T., Eugster, W., & Ojala, A. (2012) Eddy Covariance Measurements over Lakes. In M. Aubinet, T. Vesala, & D. Papale (Eds.), *Eddy Covariance* (pp. 133–157). Dordrecht: Springer Netherlands. https://doi.org/10.1007/978-94-007-2351-1_5
- 845

- Vesala, T., Huotari, J., Rannik, Ü., Suni, T., Smolander, S., Sogachev, A., ... Ojala, A. (2006). Eddy covariance measurements of carbon exchange and latent and sensible heat fluxes over a boreal lake for a full open-water period. *Journal of Geophysical Research*, *111*(D11), D11101. <https://doi.org/10.1029/2005JD006365>
- 850 Webb, E. K., Pearman, G. I., & Leuning, R. (1980). Correction of flux measurements for density effects due to heat and water vapour transfer. *Quarterly Journal of the Royal Meteorological Society*, *106*(447), 85–100. <https://doi.org/10.1002/qj.49710644707>
- Webb, J. R., Hayes, N. M., Simpson, G. L., Leavitt, P. R., Baulch, H. M., & Finlay, K. (2019). Widespread nitrous oxide undersaturation in farm waterbodies creates an unexpected greenhouse gas sink. *Proceedings of the National Academy of Sciences*, *116*(20), 9814–9819. <https://doi.org/10.1073/pnas.1820389116>
- 855 West, W. E., Coloso, J. J., & Jones, S. E. (2012). Effects of algal and terrestrial carbon on methane production rates and methanogen community structure in a temperate lake sediment: Methanogen response to trophic change. *Freshwater Biology*, *57*(5), 949–955. <https://doi.org/10.1111/j.1365-2427.2012.02755.x>
- West, W. E., McCarthy, S. M., & Jones, S. E. (2015). Phytoplankton lipid content influences freshwater lake methanogenesis. *Freshwater Biology*, *60*(11), 2261–2269. <https://doi.org/10.1111/fwb.12652>
- 860 Whalen, S. C. (2005). Biogeochemistry of methane exchange between natural wetlands and the atmosphere. *Environmental Engineering Science*, *22*(1), 73–94. <https://doi.org/10.1089/ees.2005.22.73>
- Williamson, T. J., Vanni, M. J., & Renwick, W. H. (2020). Spatial and temporal variability of nutrient dynamics and ecosystem metabolism in a hyper-eutrophic reservoir differ between a wet and dry year. *Ecosystems*. <https://doi.org/10.1007/s10021-020-00505-8>
- 865 Wik, M., Thornton, B. F., Bastviken, D., MacIntyre, S., Varner, R. K., & Crill, P. M. (2014). Energy input is primary controller of methane bubbling in subarctic lakes. *Geophysical Research Letters*, *41*(2), 555–560. <https://doi.org/10.1002/2013GL058510>
- Wik, M., Thornton, B. F., Bastviken, D., Uhlbäck, J., & Crill, P. M. (2016). Biased sampling of methane release from northern lakes: A problem for extrapolation. *Geophysical Research Letters*, *43*(3), 1256–1262. <https://doi.org/10.1002/2015GL066501>
- 870 Winslow, L., Read, J., Woolway, R., Brentrup, J., Leach, T., Zwart, J., ... Collinge, D. (2019). rLakeAnalyzer: Lake Physics Tools (Version 1.11.4.1). Retrieved from <https://CRAN.R-project.org/package=rLakeAnalyzer>

- 875 Wutzler, T., Reichstein, M., Moffat, A. M., Menzer, O., Migliavacca, M., Sickel, K., & Šigut, L. (2019). R-EddyProc: Post Processing of (Half-)Hourly Eddy-Covariance Measurements (Version 1.2). Retrieved from <https://CRAN.R-project.org/package=R-EddyProc>
- Yvon-Durocher, G., Allen, A. P., Bastviken, D., Conrad, R., Gudas, C., St-Pierre, A., ... del Giorgio, P. A. (2014). Methane fluxes show consistent temperature dependence across microbial to ecosystem scales. *Nature*, *507*(7493), 488–491. <https://doi.org/10.1038/nature13164>
- 880 Zhang, Lei, Cheng Liu, Kai He, Qiushi Shen, Jicheng Zhong, Dramatic temporal variations in methane levels in black bloom prone areas of a shallow eutrophic lake, *Science of the Total Environment*, 10.1016/j.scitotenv.2020.144868, 767, (144868), (2021).
- 885 Zhao, Y., Sherman, B., Ford, P., Demarty, M., DelSontro, T., Harby, A., ... Wu, B. (2015). A comparison of methods for the measurement of CO₂ and CH₄ emissions from surface water reservoirs: Results from an international workshop held at Three Gorges Dam, June 2012: Intercomparison of GHG measurements. *Limnology and Oceanography: Methods*, *13*(1), 15–29. <https://doi.org/10.1002/lom3.10003>

Table 1: Seasonal methane fluxes reported as mean fluxes and cumulative areal emissions from Acton Lake characterized by different measurement techniques. The eddy covariance method measures total (diffusive + ebullitive + other) fluxes.

5

Observation Type	Warm Season ¹ Mean Flux (mg CH ₄ m ⁻² hr ⁻¹)			Cumulative Annual Emissions (g CH ₄ m ⁻²)	
	Diffusive	Ebullitive	Total	Total	
2017	Eddy Covariance	--	--	9.73 ± 0.67	40.7 ± 5.9
	Shallow Site	3.2	4.47 ± 0.63	7.67 ± 0.63	29.3 ± 2.2
	Deep Site	0.89	5.76 ± 0.54	6.67 ± 0.54	29.0 ± 2.0
	Lake Surveys	1.28 ± 0.52	8.71 ± 6.1	9.98 ± 6.2	37.4 ± 5.6
	Hybrid Upscaled	--	--	10.3 ± 1.9	45.6 ± 8.3
2018	Eddy Covariance	--	--	17.5 ± 0.38	71.4 ± 4.2
	Shallow Site	3.55	5.68 ± 0.11	9.74 ± 0.11	41.9 ± 0.36
	Deep Site	0.96	6.65 ± 0.05	7.57 ± 0.05	30.8 ± 0.25
	Lake Surveys	1.87 ± 1.2	11.1 ± 6.1	13.0 ± 6.6	49.2 ± 3.7
	Hybrid Upscaled	--	--	12.9 ± 0.96	51.4 ± 4.3

¹“Warm Season” is defined as 1 May - 30 September

5

Table 2: Dissolved nutrient and carbon data for the inflow and outflow during the study period, reported as the mean of weekly samples taken between April and October, and as the value measured for the week of the 2018 spring burst (May 24 – June 4). Dissolved nutrient data includes total nitrogen (TN), ammonium (NH₄), nitrate (NO₃), total phosphorus (TP), and soluble reactive phosphorus (SRP). Dissolved carbon was measured as particulate organic carbon (POC).

Analyte (units)	2017				2018			
	Mean		Spring Burst		Mean		Spring Burst	
	Inflow	Outflow	Inflow	Outflow	Inflow	Outflow	Inflow	Outflow
TN (mg N L ⁻¹)	5.69	5.30	8.27	8.12	2.05	1.78	3.39	3.03
NH ₄ (mg N L ⁻¹)	0.05	0.07	0.02	0.02	0.05	0.05	0.17	0.07
NO ₃ (mg N L ⁻¹)	0.97	0.89	1.69	1.62	0.25	0.22	0.47	0.43
TP (µg P L ⁻¹)	115	99.9	98.6	76.6	141	80.4	254	110
SRP (µg L ⁻¹)	20.2	24.4	2.66	5.35	11.5	9.69	15.7	2.81
POC (mg L ⁻¹)	3.53	2.69	3.42	2.96	4.09	2.74	4.48	3.06

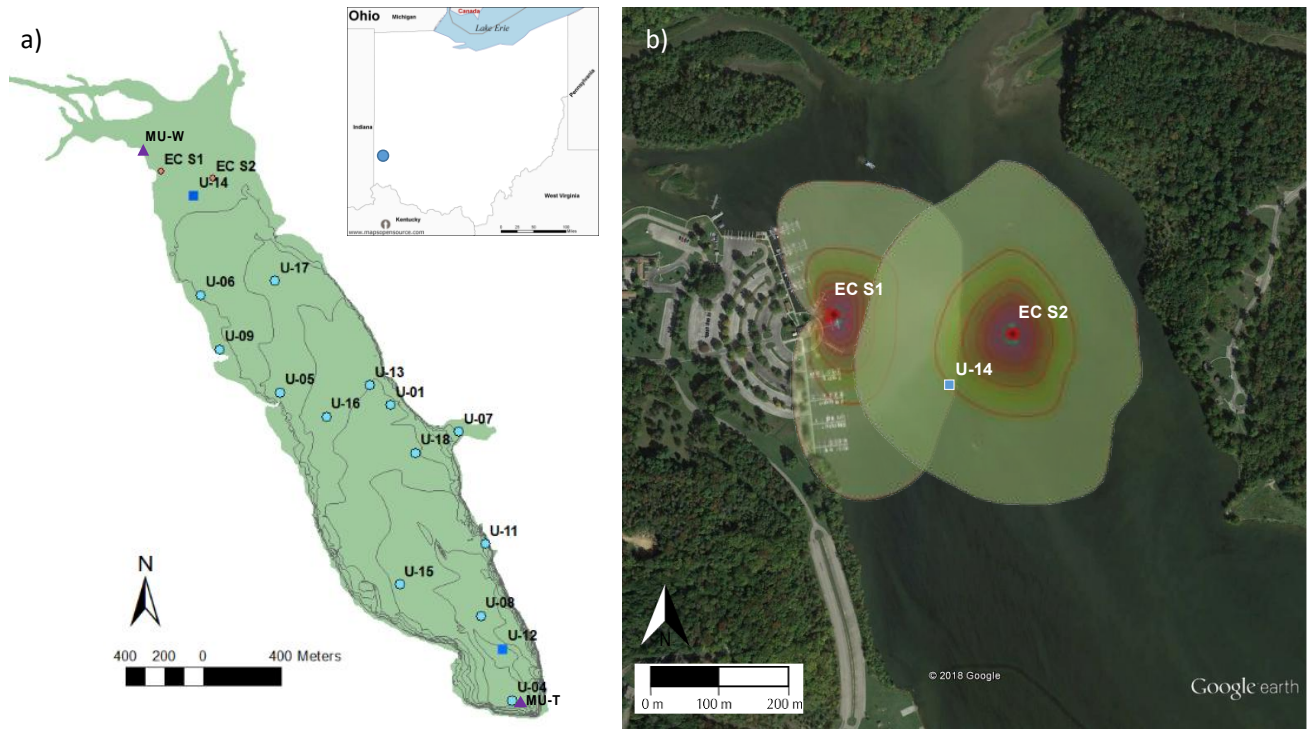
10

Table 3: Summary statistics describing the relationship between F_{CH₄} and sediment temperature per the ecoQ10 analysis and the two-dimensional Kolmogorov-Smirnov test (2DKS) threshold analysis. All

		Eddy Covariance	AFT Shallow	AFT Deep
ecoQ10	2017 value	6.96	35.1	30.4
	2017 R ²	0.85	0.48	0.60
	2018 value	5.64	35.8	30.7
	2018 R ²	0.83	0.85	0.38
Threshold (2DKS)	2017 sedT threshold	14.1	22.2	17.9
	2017 test statistic	0.226	0.166	0.204
	2018 sedT threshold	17.4	23.0	13.3
	2018 test statistic	0.234	0.190	0.138

15

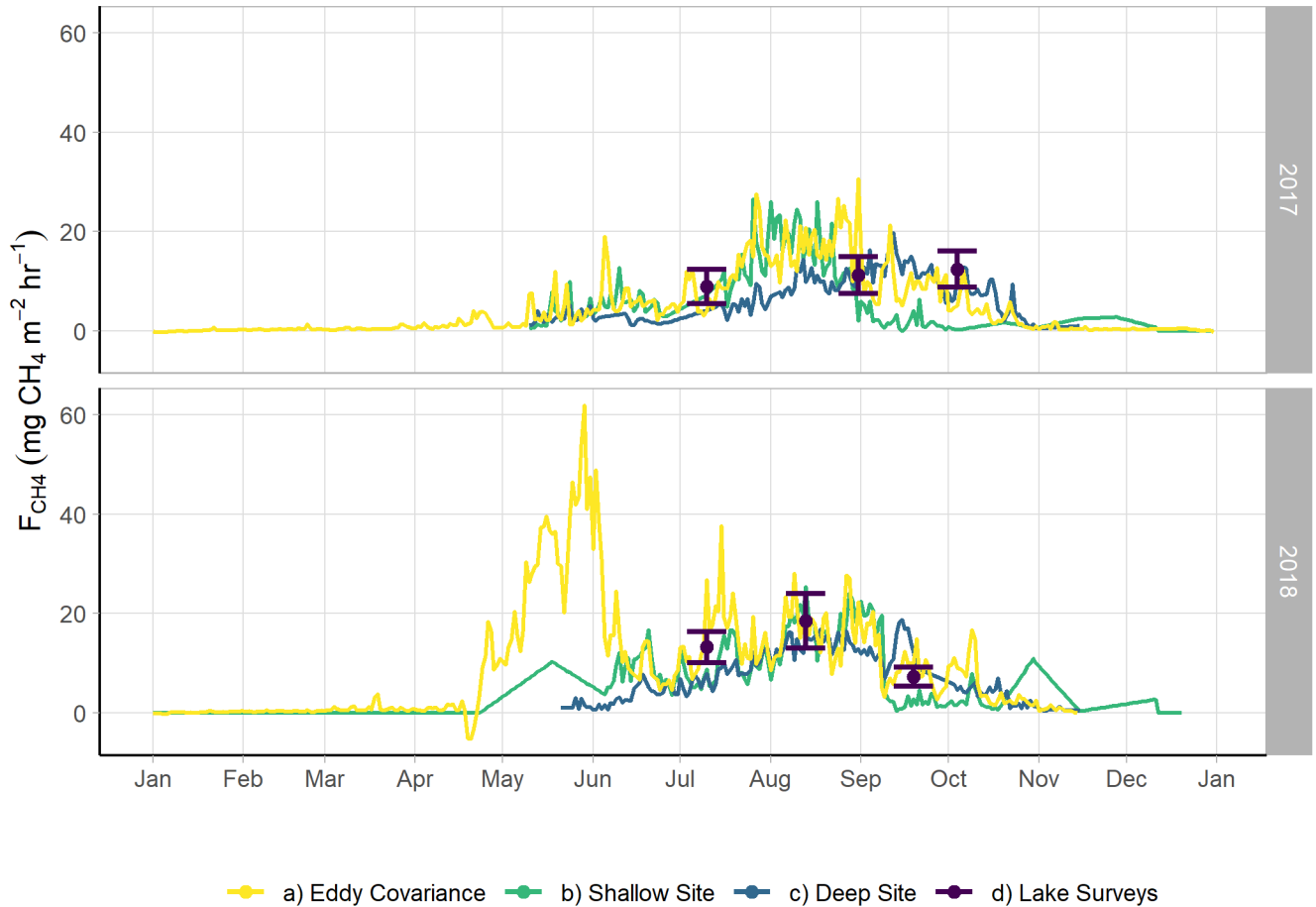
5



10

Figure 1: Map of Acton Lake (a), showing the location of multiple monitoring methods: eddy covariance flux tower sites (red circles), active funnel traps and bi-weekly chamber measurements (dark blue squares), and spatially extensive survey sites (light blue circles), and the weather station and thermistors operated by Miami University (purple triangles). The lake contour lines represent ~1m depth increments. Inset image shows the location of Acton Lake in southwest Ohio. The Google Earth image (b) shows the 80% cumulative footprint probability distribution at each eddy covariance flux tower site at 10% intervals

15



5 **Figure 2: Time series of F_{CH_4} monitored via multiple methods: eddy covariance (violet), the sum of the shallow AFT and interpolated chamber measurements (blue, site U-14), the sum of the deep AFT and interpolated chamber measurements (green, site U-12), and via the spatially integrated lake-wide surveys (yellow). The error bars for the lake surveys indicate the 95% confidence interval of the mean. Error margins for the other measurements are omitted for figure legibility. The spring burst period was 24 May - 4 June 2018.**

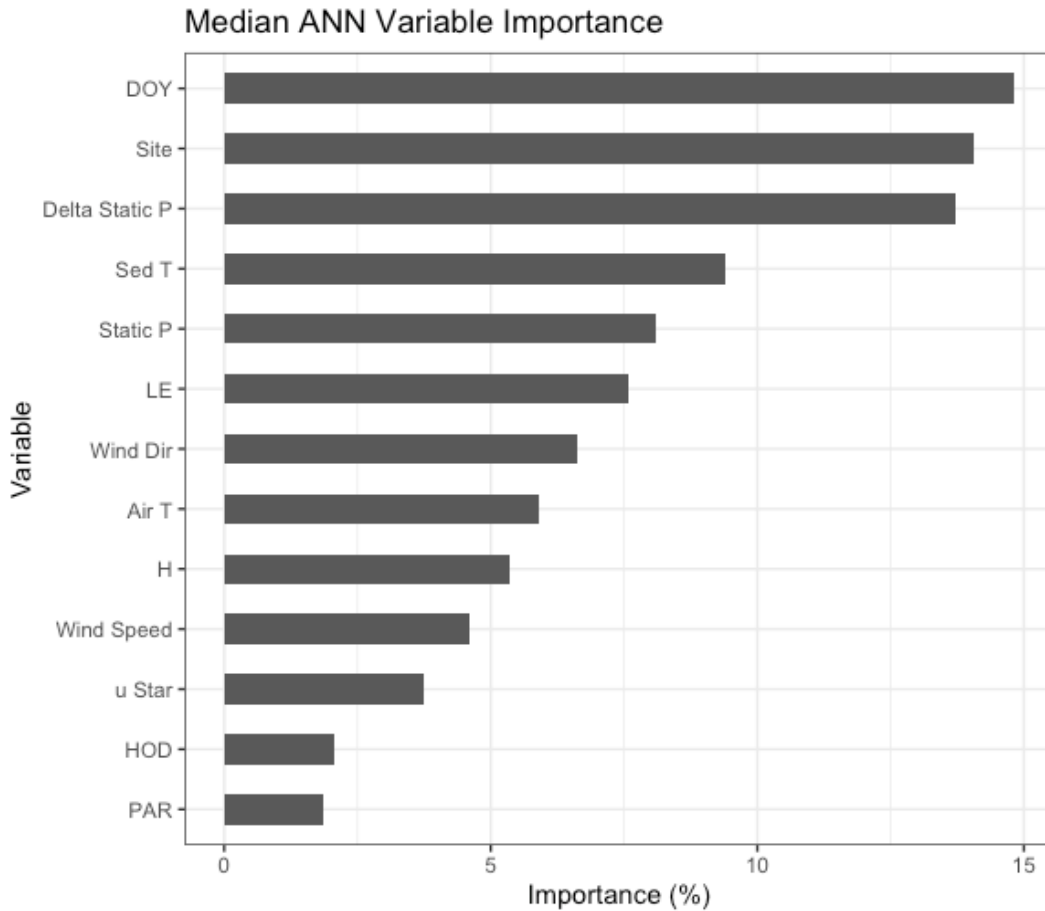
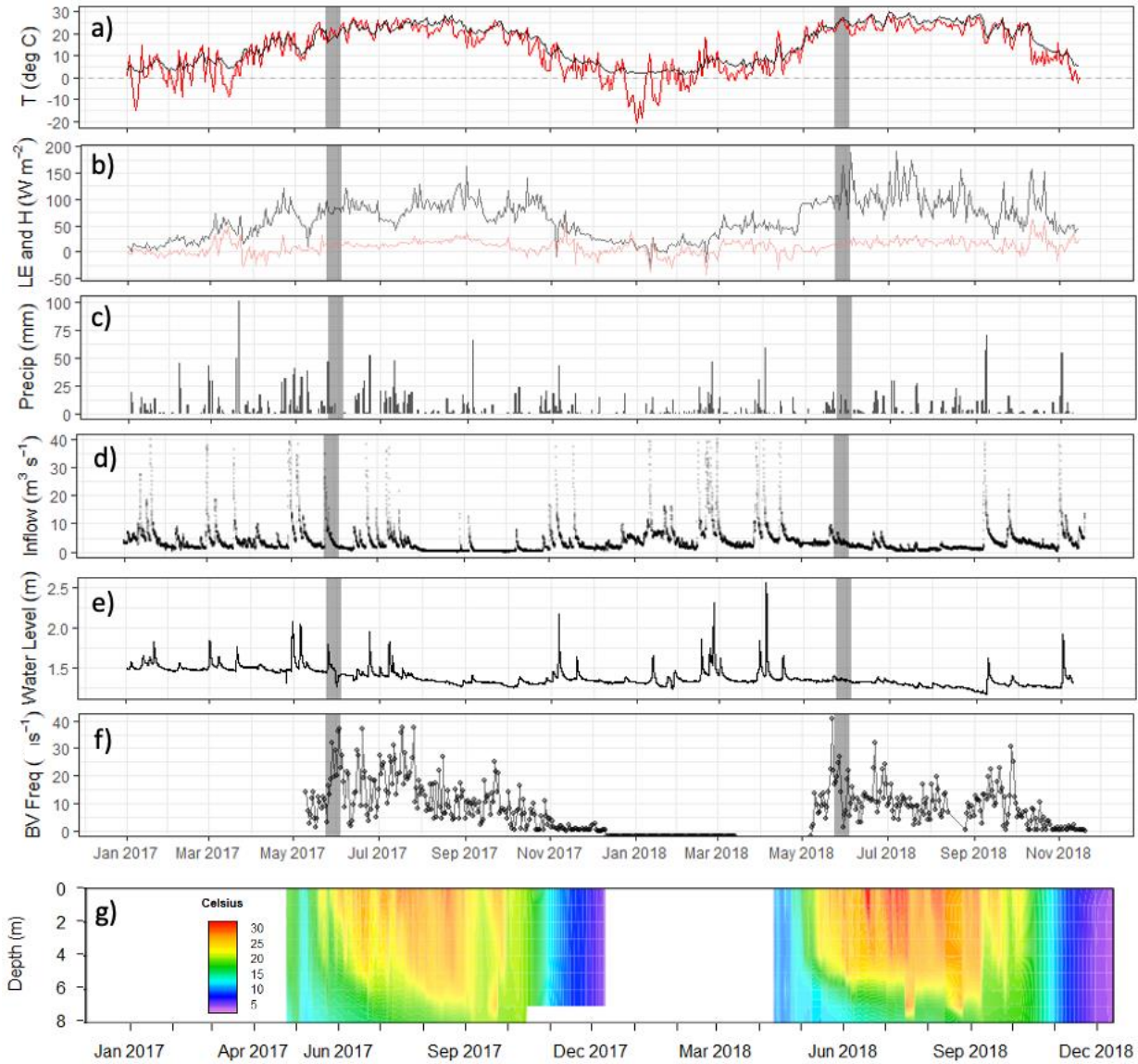


Figure 3: Median variable importance ranking for the drivers of the artificial neural network gap-filling model in terms of percent importance to the predictive power of the model. This ranking is based both on intra-model variability (i.e. the effect of model architecture and random seed selection) and on inter-model variability (i.e. the effect of data selection for the training, testing, and validation datasets). DOY = day of year; Delta static P is change in overlying static pressure; Sed T is sediment temperature, LE is latent heat flux; Static P is static pressure; Wind Dir is wind direction; H is sensible heat flux; u Star is friction velocity; PAR is photosynthetically active radiation; HOD is hour of day.

5



5 **Figure 4: Meteorological and limnological conditions over the study period: (a) daily mean of air (red) and sediment (black) temperature; (b) daily mean latent and sensible heat fluxes (LE, black, and H, red, respectively); (c) daily cumulative precipitation (mm); (d) stream inflow ($\text{m}^3 \text{s}^{-1}$); (e) water depth in the footprint of the flux tower (m); (f) Brunt Väisälä frequency, a measure of water column mixing potential (s^{-1}); and (g) the water temperature profile at the deep site (U-12). Grey bars indicate the time frame of the 2018 spring burst of CH_4 emissions.**

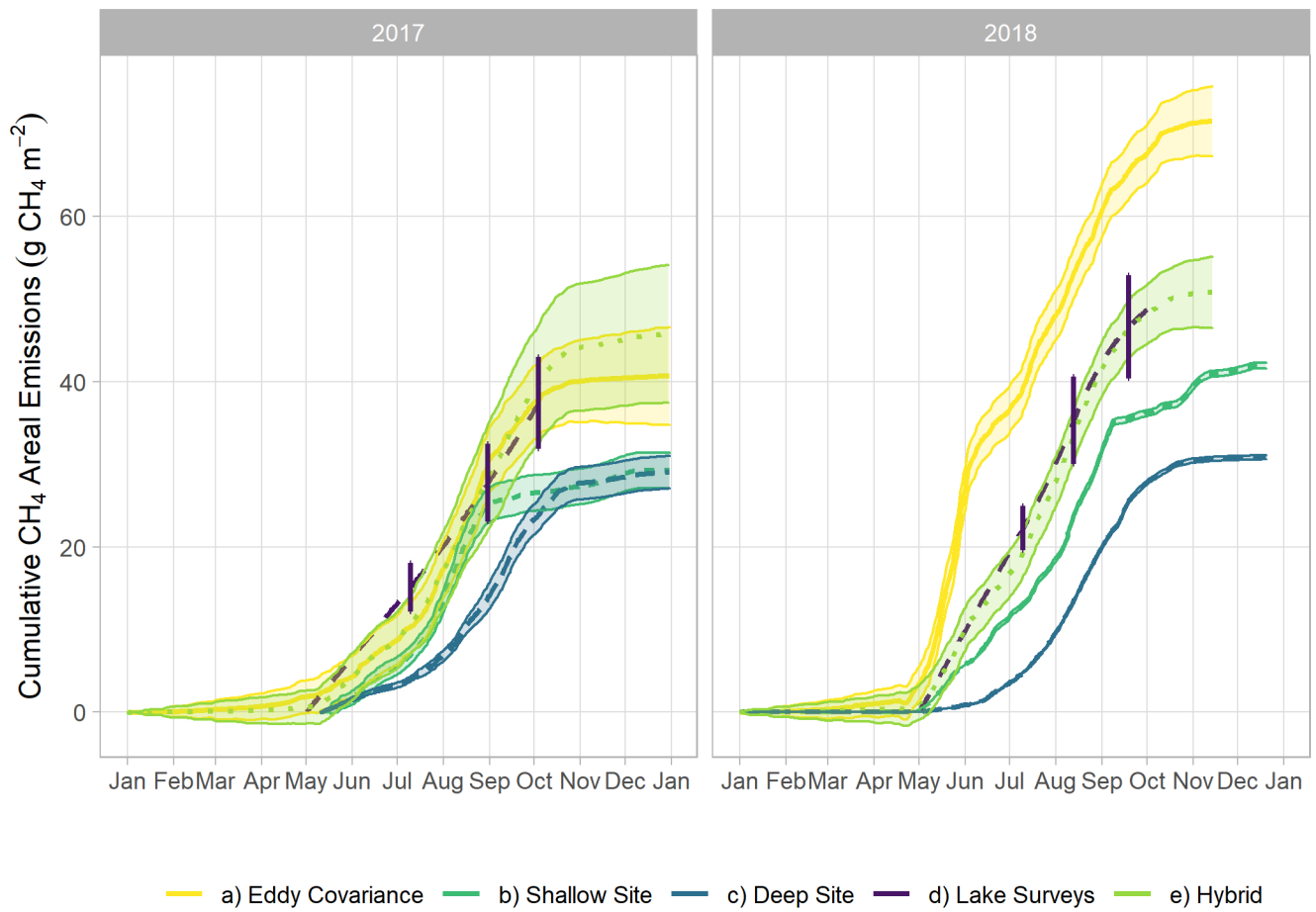


Figure 5: Cumulative areal emissions in 2017 and 2018 from EC, sum of AFT and chamber, spatial survey monitoring, and hybrid upscaling results (g CH₄ m⁻²). Vertical lines intersecting the Lake Survey trace represent the 95% confidence interval of the lake-wide F_{CH₄} estimate.

5

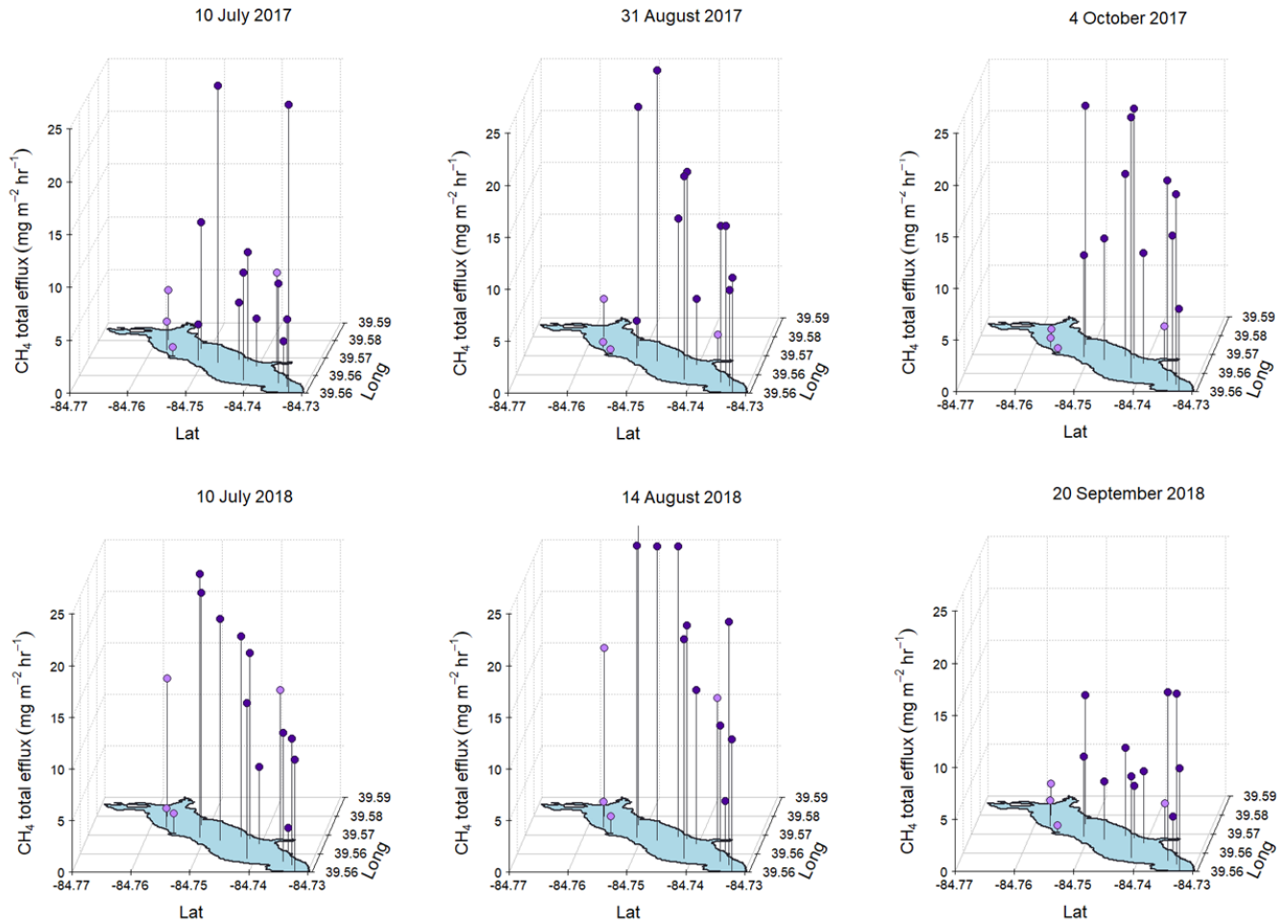


Figure 6: Total (ebullitive + diffusive) F_{CH_4} measured during mid-summer, late-summer, and fall spatial surveys at Acton Lake during 2017 (top row) and 2018 (bottom row). Dots indicate magnitude of F_{CH_4} per the z-axis scale and vertical black lines connect red dots to their corresponding sampling location. Dot color indicates whether a sampling site is in the shallow (< 3 m, lavender) or deep (> 3 m, royal purple) area of the reservoir.

5

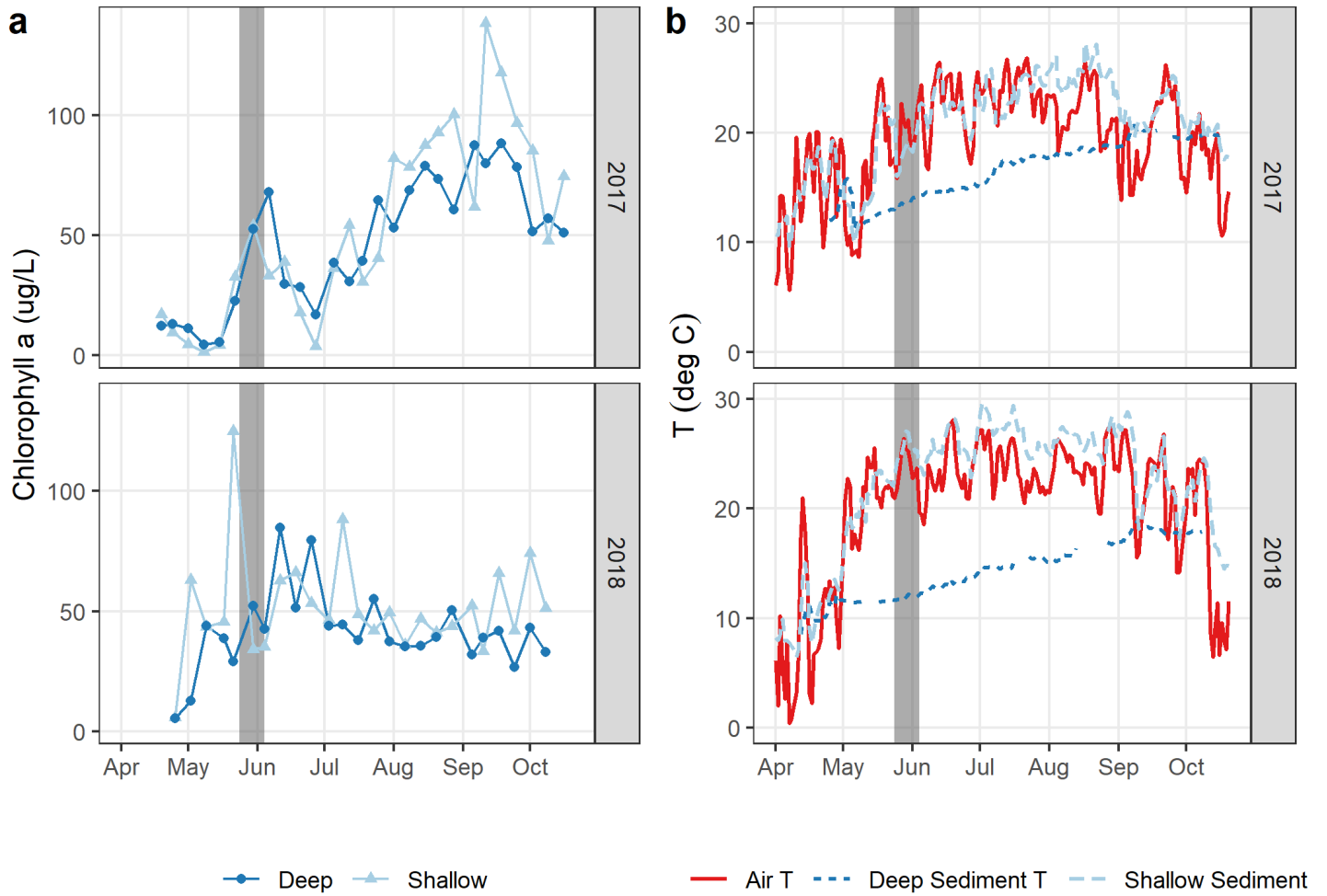


Figure 7: Daily air and sediment temperature (a, left) and chlorophyll a (an indicator for algal biomass, b, right) in 2017 and 2018. The grey bar indicates the spring burst period of elevated F_{CH_4} in 2018, likely supported by elevated sediment temperature and algal biomass levels that year.

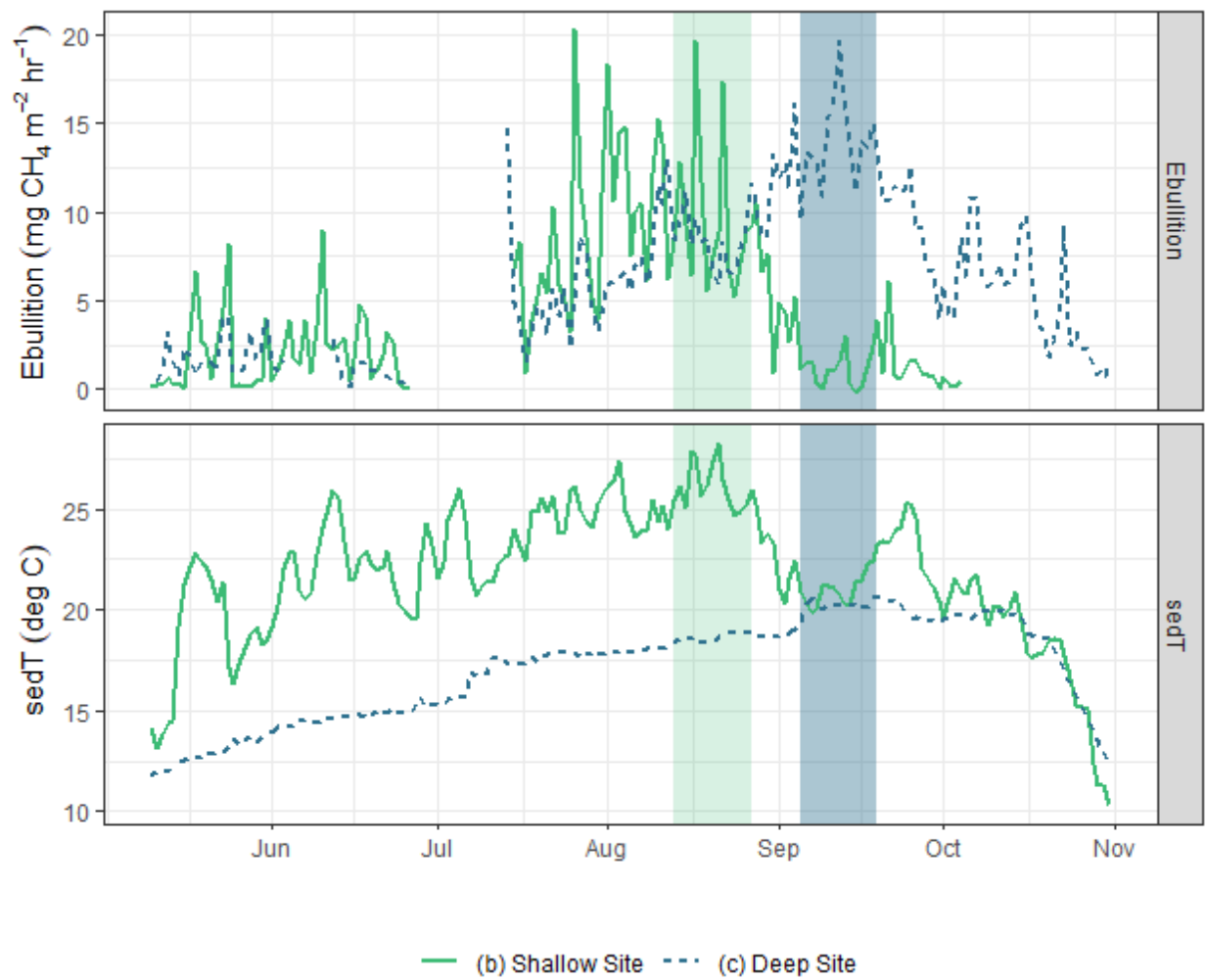


Figure 8: Time series of sedT and ebullition in 2017 at the shallow (green solid line) and deep (blue dashed line) sites. The light grey bar highlights the period of maximum ebullition and sedT at the shallow site; the dark grey bar highlights the corresponding period at the deep site.